



# CHORUS

This is the accepted manuscript made available via CHORUS. The article has been published as:

## Ultimate capabilities for compression of the waveform of a recoilless $\gamma$ -ray photon into a pulse sequence in an optically deep vibrating resonant absorber

I. R. Khairulin, V. A. Antonov, Y. V. Radeonychev, and Olga Kocharovskaya

Phys. Rev. A **98**, 043860 — Published 31 October 2018

DOI: [10.1103/PhysRevA.98.043860](https://doi.org/10.1103/PhysRevA.98.043860)

# Ultimate capabilities for compression of the waveform of recoilless $\gamma$ -ray photon into a pulse sequence in an optically deep vibrating resonant absorber

I. R. Khairulin<sup>1,2</sup>, V. A. Antonov<sup>2,3,\*</sup>, Y. V. Radeonychev<sup>2,1</sup>, and Olga Kocharovskaya<sup>4</sup>

<sup>1</sup> *N.I. Lobachevsky State University of Nizhny Novgorod,  
23 Gagarin Avenue, Nizhny Novgorod, 603950, Russia,*

<sup>2</sup> *Institute of Applied Physics of the Russian Academy of Sciences,  
46 Ulyanov Street, Nizhny Novgorod, 603950, Russia,*

<sup>3</sup> *Prokhorov General Physics Institute of the Russian Academy of Sciences,  
38 Vavilov Street, Moscow, 119991, Russia,*

<sup>4</sup> *Department of Physics and Astronomy and  
Institute for Quantum Studies and Engineering,  
Texas A&M University, College Station, TX 77843-4242, USA.*

Recently, an exponentially decaying waveform (the time-dependence of detection probability) of a Mössbauer  $\gamma$ -ray photon was transformed into a regular sequence of short pulses in a sinusoidally vibrating recoilless resonant absorber [*Nature*, **508**, 80-83 (2014)]. In the present paper, we show that the peak amplitude of the pulses can be considerably increased via joint adjustment of optical depth of the absorber and the initial phase of its vibration. This is due to reduction of the photoelectric absorption and maximizing the constructive temporal interference of spectral content of the single-photon wave packet in optically deep absorber. The ultimate capabilities for transforming a waveform of 14.4 keV photon from <sup>57</sup>Co radioactive source into a regular train of pulses in a harmonically vibrating <sup>57</sup>Fe recoilless resonant absorber are discussed. We show that the shortest pulse duration, produced by this technique, is limited by the highest available vibration frequency of a piezo-transducer and at present can be as short as 7.7 ps. The maximum achievable detection probability of the transformed photon at the experimentally feasible conditions is more than two times higher than peak detection probability of the photon emitted by the source and nearly 5.5 times higher than obtained in the above reference.

## I. INTRODUCTION

Hard x-ray/ $\gamma$ -ray optics is an attractive and rapidly growing branch of physics, which gives rise to numerous applications in material science, chemistry, biology, medicine and modern technologies. Extremely short wavelengths of hard x-ray/ $\gamma$ -ray photons allow investigating material structure at atomic scales, while narrow bandwidth of Mössbauer radiation (for example, a bandwidth of emission of <sup>57</sup>Co radioactive source with photon energy 14.4 keV is  $\sim 1$  MHz, which corresponds to  $3 \times 10^{-12}$  of its carrier frequency) permits precise measurements of local electric and magnetic fields, energy structure and hyperfine interactions in solids and on their surfaces.

In recent years, a growing interest to these studies was motivated by penetration of concepts and ideas of coherent and quantum optics into x-ray range of electromagnetic spectrum. Earlier experimental achievements in this field include demonstrations of the Autler-Townes effect [1],  $\gamma$ -ray echo via abrupt shift of a nuclear absorber [2], controllable storage and release of nuclear excitation by switch of the magnetic field direction [3], electromagnetically induced transparency (EIT) via a nuclear level anti-crossing [4], slowing down of  $\gamma$ -photon in a nuclear absorber with a split line [5] and other effects discussed in the review [6]. Recent experimental advances include demonstration of parametric down-conversion in the Langevin regime [7], cav-

ity electromagnetically induced transparency [8], collective Lamb shift [9], vacuum-assisted generation of atomic coherences [10], single-photon revival in nuclear absorbing sandwiches [11], phase-sensitive measurements characterizing the quantum state of a nuclei at hard x-ray energies [12], and group velocity control for 14.4 keV-energy photons [13], spectral enhancement of x-ray radiation via a moving absorber [14] and demonstration of a strong coupling between two nuclear polariton modes [15]. Also, a number of important effects were theoretically predicted recently including dynamical control of x-ray polarization qubits by nuclear Mössbauer resonance [16], heralded entanglement between two crystal-hosted macroscopic nuclear ensembles [17], as well as mapping and storing x-ray pulses in a thin-film planar x-ray cavity with embedded resonant nuclear medium [18].

Recently, a possibility for coherent manipulation of the waveform (the time-dependence of detection probability) of Mössbauer  $\gamma$ -ray photon in a harmonically vibrating recoilless resonant absorber was shown both theoretically and experimentally [19]. In particular, (i) transformation of the exponentially decaying waveform of an incident 14.4 keV photon into a regular sequence of nanosecond pulses, and (ii) splitting of a single  $\gamma$ -ray photon into double-spike pulse were shown. However, in the proof-of-principle experiment [19] neither the absorber optical depth, nor the initial phase of its vibration (the phase of vibration at the moment, when the front of the single-photon wave packet enters the medium) were optimized.

Further development of this approach was presented in [20], where an analytical solution was derived for the waveform of a  $\gamma$ -ray photon transmitted through the vibrating recoilless resonant absorber under the conditions realized in [19]. It was shown that bunches of predetermined number of pulses can be produced, and the possibilities for using them in quantum information processing were discussed. The theoretical results were confirmed experimentally.

In the following papers [21] and [22], transformation of a continuous flow of  $\gamma$ -ray photons emitted by a high-activity source into a periodic pulse train was considered. In those papers, the possibilities to improve the peak intensity, duration and shape of pulses with respect to the proof-of-principle experiment [19] were discussed. It was proposed (i) to increase an optical depth of the resonant absorber [22], and (ii) to use several sequentially placed resonant absorbers [21]. In particular, a possibility to increase the pulse peak intensity due to phase-matching of the vibrational sidebands of  $\gamma$ -radiation via the absorber dispersion was discussed [21, 22].

Nevertheless, the optimal conditions for transformation of a single-photon waveform into a train of pulses taking into account propagation effects in optically deep medium were not analyzed yet. At the same time, it is well known that in optically deep absorber the exponentially decaying waveform of a photon transforms into a sequence of dips and humps, which is called "dynamical beats", and originates from spectrally-selective interaction of the photon field with the resonant nuclei [23]. With increasing absorber optical depth the dynamical beats shrink towards the front of the photon waveform (the dips and humps alternate faster). If the absorber vibrates under the conditions realized in [19], the produced pulses interfere with the dynamical beats. As a result, some of the pulses can be enhanced or suppressed. As shown in [19], the initial phase of absorber's vibration determines position of the pulses in respect to the front of the waveform, and hence to the dynamical beats. Therefore, tuning both the initial phase of vibration and the optical depth of absorber allows matching one or several pulses arisen due to vibration with dynamical beats. As shown below, such a constructive interference can noticeably enlarge the pulse height.

In the present paper we study the possibilities to improve characteristics of pulses, which are produced from a single-photon waveform in a vibrating recoilless resonant absorber, via joint

optimization of (i) the optical depth of absorber responsible for the dynamical beats, and (ii) the initial phase of vibration determining position of the produced pulses with respect to dynamical beats. We also consider the possibility to use resonant dispersion of the absorber for increasing the pulse intensity in the single-photon regime.

The paper is organized as follows. In Section II we present the theoretical model. In Sec. III we derive an analytical solution for this model describing transformation of the exponentially decaying waveform of a Mössbauer photon into a regular sequence of short pulses taking into account propagation effects in optically deep recoilless resonant absorber. On the basis of this solution we discuss physical mechanisms which allow increasing the pulse height. In Sec. IV we find analytically and numerically the optimal parameter values for maximizing the peak detection probability of the photon for feasible experimental conditions, including conditions for producing the shortest pulses and conditions of the proof-of-principle experiment [19]. In Sec. V we discuss another physical mechanisms leading to enhancement in the temporal detection probability. In Sec. VI we summarize the results.

## II. THEORETICAL MODEL

Let us consider transformation of a 14.4 keV photon, emitted by  $^{57}\text{Co}$  Mössbauer radioactive source, in a recoilless  $^{57}\text{Fe}$  resonant absorber, oscillating along the direction of propagation of Mössbauer radiation. The relevant energy levels of the source are shown in a left side of Fig.1a. The  $^{57}\text{Co}$  radioactive nuclide decays via electron capture producing a  $^{57}\text{Fe}$  nucleus in the state  $|c\rangle$  which decays with lifetime  $T_c \approx 12$  ns to the state  $|b\rangle$ , emitting a 122 keV  $\gamma$ -ray photon. Subsequently, the state  $|b\rangle$  decays with lifetime  $T_s \approx 141$  ns to the ground state  $|a\rangle$ , emitting a 14.4 keV photon. Detection of 122 keV photon determines the instant of formation of the state  $|b\rangle$ . It is chosen to be a time origin,  $t_0=0$ , for the time dependence of probability for detecting the 14.4 keV photon,  $N_s(t)$ , that is proportional to the coincidence count rate of the 14.4 keV photons emitted from the source,

$$N_s(t) = \frac{1}{T_s} \theta(t) \exp\{-t/T_s\}, \quad (1)$$

where  $\theta(t)$  is the unit step function and  $T_s$  is the decay time of the state  $|b\rangle$ . After pass through a diaphragm, viewed in a small solid angle, the electric field of the photon can be represented in the form [23-27] (Fig.1b, upper part):

$$E_s(\tau_{lab}) = \frac{1}{2} E_0 \theta(\tau_{lab}) e^{-i(\omega_s + \Gamma_s/2)\tau_{lab} + i\varphi_0} + \text{c.c.}, \quad (2)$$

where  $E_0$  is the field amplitude,  $\tau_{lab} = t - z_{lab}/c$  is the local time in the laboratory reference frame,  $z_{lab}$  is the coordinate along the direction of the field propagation in the laboratory reference frame,  $\Gamma_s = 1/T_s$  is the radiation bandwidth (for  $^{57}\text{Fe}$  nuclide  $\Gamma_s/(2\pi) \approx 1.13$  MHz,  $\omega_s$  is the carrier frequency of the field corresponding to the wavelength  $\lambda_s \approx 0.86$  Å,  $\varphi_0$  is the random initial phase of the field, and c.c. stands for complex conjugation. In Eq. (2) we neglected (i) the value  $z_s/c$  (where  $z_s = z_0 + V_s t$  is the coordinate of the emitting nucleus that can be moved with constant velocity  $V_s$ , Fig. 1b) in the argument of unit step function and (ii) the value  $\Gamma_s z_s/(2c)$  in

the exponent of the exponential function. Both approximations are valid at the propagation distances  $z_s \ll 2c/\Gamma_s$  (in the case of  $^{57}\text{Fe}$ ,  $2c/\Gamma_s \approx 84.5$  m).

Let us consider propagation of the photon through the resonant absorber. The absorber constitutes a foil of stainless steel enriched by the resonant  $^{57}\text{Fe}$  nuclei (Fig.1a right side), fixed on a piezoelectric plate and vibrating piston-like with frequency  $\Omega$  along the direction of the photon propagation (Fig.1b). The thickness of the film,  $L$ , satisfies the inequality  $L \ll 2\pi V_{\text{sound}}/\Omega$ , where  $V_{\text{sound}}$  is the speed of sound in stainless steel. Consequently, the absorber vibrates as a whole according to

$$z_{\text{lab}} = z_a + R \sin(\Omega t + \mathcal{G}_0), \quad (3)$$

where  $z_a$  is the coordinate in the vibrating reference frame,  $R$  is the amplitude and  $\mathcal{G}_0$  is the initial phase of absorber's vibration. The absorber's motion is nonrelativistic,  $R\Omega \ll c$  (where  $c$  is the speed of light in vacuum), therefore time in the vibrating reference frame is the same as in the laboratory reference frame. Substituting (3) into (2) allows one to write the electric field of emitted photon in the vibrating reference frame as a frequency-modulated field,

$$E_s(\tau_a, t) = \frac{1}{2} E_0 \theta(\tau_a) e^{-\Gamma_s \tau_a / 2} e^{-i[\omega_s \tau_a - p \sin(\Omega \tau_a + \mathcal{G}_0) - \varphi_0]} + \text{c.c.}, \quad (4)$$

where  $\tau_a = t - z_a/c$  is the local time in the vibrating reference frame, and  $p = 2\pi R/\lambda_s$  is the index of modulation of the resonant transition frequency. In Eq. (4) we neglected both sinusoidal term in step function and amplitude modulation of the photon field, because of nonrelativistic motion of the absorber. According to (4), in the reference frame of the vibrating absorber the field of the incident photon acquires harmonic frequency modulation with a modulation frequency  $\Omega$ . We assume that there is no reflection of the field from the absorber's surface since the dielectric permittivity of the absorber's material in the  $\gamma$ -ray range is very close to unity. Therefore in the vibrating reference frame at the entrance to the absorber,  $z_a = 0$ , the frequency-modulated photon field coincides with the emitted field (4) and can be represented in the form

$$E_{\text{inc}}(\tau_a) = \frac{1}{2} A_{\text{inc}}(\tau_a) e^{-i\omega_s \tau_a} + \text{c.c.}, \quad (5a)$$

$$A_{\text{inc}}(\tau_a) = E_0 e^{i\varphi_0} \theta(\tau_a) \exp\{-\Gamma_s \tau_a / 2\} \exp\{ip \sin(\Omega \tau_a + \mathcal{G}_0)\}, \quad (5b)$$

where  $A_{\text{inc}}(\tau_a)$  is the slowly-varying complex amplitude of the incident field,  $|dA_{\text{inc}}/d\tau_a| \ll \omega_s |A_{\text{inc}}|$ . Using the Jacobi-Anger expansion, the incident field can be considered as a single-photon wave packet composed of a set of the exponentially decaying spectral components with equidistant carrier frequencies (Fig.1b, lower part),

$$E_{\text{inc}}(\tau_a) = \frac{1}{2} \sum_{n=-\infty}^{\infty} \theta(\tau_a) E_0 J_n(p) e^{-\Gamma_s \tau_a / 2} e^{-i[(\omega_s - n\Omega)\tau_a - n\mathcal{G}_0 - \varphi_0]} + \text{c.c.}, \quad (5c)$$

where  $J_n(p)$  is the Bessel function of the first kind of order  $n$ . Applying Fourier transform to

equation (5b),  $A_{\text{inc}}(\omega) = \frac{1}{2\pi} \int_{-\infty}^{\infty} A_{\text{inc}}(\tau_a) e^{i\omega \tau_a} d\tau_a$ , one gets complex amplitude of a monochromatic

frequency constituent of the single-photon wave packet:

$$A_{\text{inc}}(\omega) = \frac{E_0}{2\pi} \sum_{n=-\infty}^{\infty} \frac{J_n(p) e^{i(\varphi_0 - n\mathcal{G}_0)}}{-i(\omega - n\Omega) + \Gamma_s / 2}, \quad (5d)$$

As follows from (5d), in the reference frame of the vibrating absorber the quasi-monochromatic incident field (2) can be considered as a comb of equidistant spectral components separated by the frequency of vibration. The  $n^{\text{th}}$  component has the central frequency  $\omega_n = \omega_s + n\Omega$ , relative amplitude  $|J_{-n}(p)|$ , and Lorentz shape with bandwidth  $\Gamma_s$ . The phase at its central frequency,  $\omega_n$ , at  $\tau_a = 0$  will be referred below as the central phase of the  $n^{\text{th}}$  spectral component. For a fixed value of modulation index,  $p$ , there are approximately  $2p+1$  spectral components with considerably nonzero amplitudes.

Interaction of the photon with a resonant nuclear transition from the ground state,  $|1\rangle$ , to the excited state,  $|2\rangle$ , of  $^{57}\text{Fe}$  nuclei of the absorber (Fig.1a, right side) can be described by a master equation for the quantum coherence between these states,  $\rho_{21}$ , [19, 25-27]

$$\frac{d\rho_{21}}{dt} + (i\omega_a + \gamma_a)\rho_{21} = in_{12} \frac{d_{21}E}{\hbar}, \quad (6)$$

where  $\omega_a$  is the frequency of the resonant transition  $|1\rangle \leftrightarrow |2\rangle$ , which can differ from the central frequency of the source,  $\omega_s$ , due to isomeric shift or Doppler shift produced by a motion of the absorber relative to the source with a constant velocity  $V_s$  (Fig.1b),  $\gamma_a$  is the half-width of spectral line of the resonant transition,  $n_{12} = \rho_{11} - \rho_{22}$  is the population difference between the states  $|1\rangle$  and  $|2\rangle$ ,  $d_{21}$  is the dipole moment of the resonant transition,  $E$  is the electric field of the photon inside the medium, and  $\hbar$  is the Plank's constant. Excitation of the quantum coherence,  $\rho_{21}$ , results in resonant macroscopic polarization of the medium,

$$P = f_a N d_{12} \rho_{21} + \text{c.c.}, \quad (7)$$

where  $f_a$  is the Lamb-Mössbauer factor (probability of Mössbauer effect) in the absorber's material,  $N$  is the concentration of the resonant nuclei, and  $d_{12} = d_{21}^*$ . In its turn, the resonant polarization of the medium,  $P$ , leads to transformation of the photon field,  $E$ , in accordance with the wave equation

$$\frac{\partial^2 E}{\partial z_a^2} - \frac{1}{c'^2} \frac{\partial^2 E}{\partial t^2} = \frac{2\delta_e}{c'} \frac{\partial E}{\partial t} + \frac{4\pi}{\varepsilon c'^2} \frac{\partial^2 P}{\partial t^2}, \quad (8a)$$

where  $\varepsilon$  is the nonresonant dielectric permittivity of the absorber's material,  $c' = c/\sqrt{\varepsilon}$  is the speed of light in the medium, and  $\delta_e$  is the photoelectric absorption coefficient.

Let us change the independent variables from  $(z_a, t)$  to  $(z_a, \tau'_a)$ , where  $\tau'_a = t - z_a/c'$ . In such a case, wave equation (8a) takes the form

$$\frac{\partial^2 E}{\partial z_a^2} - \frac{2}{c'} \frac{\partial^2 E}{\partial z_a \partial \tau'_a} = \frac{2\delta_e}{c'} \frac{\partial E}{\partial \tau'_a} + \frac{4\pi}{\varepsilon c'^2} \frac{\partial^2 P}{\partial \tau_a'^2}, \quad (8b)$$

while equation for the quantum coherence (6) retains its form except for the replacement  $t \rightarrow \tau'_a$ . Let us further use approximation of the slowly-varying complex amplitude:

$$\begin{cases} E(z_a, \tau'_a) = \frac{1}{2} \tilde{E}(z_a, \tau'_a) e^{-i\omega_s \tau'_a} + \text{c.c.}, \\ P(z_a, \tau'_a) = \frac{1}{2} \tilde{P}(z_a, \tau'_a) e^{-i\omega_s \tau'_a} + \text{c.c.}, \\ \rho_{21}(z_a, \tau'_a) = \tilde{\rho}_{21}(z_a, \tau'_a) e^{-i\omega_s \tau'_a}, \end{cases} \quad (9)$$

where  $|\partial \tilde{F} / \partial \tau'_a|$ ,  $c' |\partial \tilde{F} / \partial z_a| \ll \omega_s |\tilde{F}|$ , and  $\tilde{F}$  stands for  $\tilde{E}$ ,  $\tilde{P}$ , and  $\tilde{\rho}_{21}$ . This approximation is well satisfied in the considered case, since  $\omega_s \gg \Gamma_s, p\Omega$ . Under this approximation the wave equation (8b) takes the form

$$\frac{\partial \tilde{E}}{\partial z_a} + \delta_e \tilde{E} = i \frac{2\pi\omega_s}{\varepsilon c'} \tilde{P}, \quad (10)$$

where we took into account that  $\delta_e \ll \omega_s / c'$ . Eq. (6) takes the form

$$\frac{d \tilde{\rho}_{21}}{d \tau'_a} + (i[\omega_a - \omega_s] + \gamma_a) \tilde{\rho}_{21} = in_{12} \frac{d_{21} \tilde{E}}{2\hbar}, \quad (11)$$

which also implies the rotating-wave approximation,  $|\omega_a - \omega_s| \ll \omega_s$ , while relation between the amplitudes of quantum coherence and macroscopic polarization (7) is given by

$$\tilde{P} = 2f_a N d_{12} \tilde{\rho}_{21}. \quad (12)$$

Let us seek for a solution of the system (10)-(12) in the form

$$\tilde{F}(z_a, \tau'_a) = \int_{-\infty}^{\infty} \tilde{F}(z_a, \omega) e^{-i\omega \tau'_a} d\omega, \quad (13a)$$

where  $\tilde{F}$  stands for  $\tilde{E}$ ,  $\tilde{P}$ , and  $\tilde{\rho}_{21}$ ; and further

$$\tilde{F}(z_a, \omega) = \tilde{F}_0(\omega) \exp\{-(\delta_e + g(\omega))z_a\}. \quad (13b)$$

Eqs. (10)-(13) give us

$$g(\omega) = \frac{2\pi f_a n_{12} N |d_{12}|^2 \omega_s}{\hbar c \sqrt{\varepsilon} [\gamma_a + i(\omega_a - \omega_s - \omega)]}. \quad (14)$$

In its turn, the value of  $\tilde{E}_0(\omega)$  is determined from the boundary condition at the front edge of the medium,  $z_a = 0$ , which is  $\tilde{E}_0(\omega) = A_{inc}(\omega)$ , where  $A_{inc}(\omega)$  is determined by Eq. (5d). Consequently, we find the slowly-varying amplitude of the single-photon wave packet inside the medium in the form

$$\tilde{E}(z_a, \tau'_a) = \frac{E_0}{2\pi} e^{-\delta_e z_a} \sum_{n=-\infty}^{\infty} J_n(p) e^{i(\varphi_0 + n\vartheta_0)} \int_{-\infty}^{\infty} \frac{\exp\{-g(\omega)z_a - i\omega \tau'_a\}}{-i(\omega + n\Omega) + \Gamma_s/2} d\omega. \quad (15)$$

Its intensity behind the absorber is  $I_{out}(\tau_a) = \frac{c}{8\pi} |\tilde{E}(z_a = L, \tau_a)|^2$  where  $\tau'_a$  in (15) is replaced with  $\tau_a$ .

Let us return to the laboratory reference frame and look for the field of the photon behind the absorber in the form

$$E_{out}(\tau_{lab}) = \frac{1}{2} A_{out}(\tau_{lab}) e^{-i\omega_s \tau_{lab}} + \text{c.c.}, \quad (16)$$

where  $\tau_{lab} = t - z_{lab}/c$ , and  $A_{out}$  is the slowly-varying amplitude of the output field. The substitution  $\tau_{lab} \rightarrow \tau_a \rightarrow \tau'_a$ , and use of the boundary condition in the form  $E_{out}(\tau'_a) = E(z_a = L, \tau'_a)$  results in

$$A_{out}(\tau_{lab}) = \frac{E_0}{2\pi} e^{-\delta_e L} \exp\{-ip \sin(\Omega \tau_{lab} + \mathcal{G}_0)\} \sum_{n=-\infty}^{\infty} J_n(p) e^{i(\varphi'_0 + n\vartheta_0)} \int_{-\infty}^{\infty} \frac{\exp\{-g(\omega)L - i\omega\tau_{lab}\}}{-i(\omega + n\Omega) + \Gamma_s/2} d\omega, \quad (17)$$

where  $\varphi'_0 = \varphi_0 + \Delta\varphi_0$ . and  $\Delta\varphi_0 = i \frac{\omega_s}{c} L (\sqrt{\varepsilon} - 1)$ .

The time-dependent probability of the photon detection behind the absorber can be described in terms of intensity of the output field,  $N_{out}(\tau_{lab}) \propto I_{out}(\tau_{lab}) = \frac{c}{8\pi} |A_{out}(\tau_{lab})|^2$ . From Eq. (17) we get

$$I_{out}(\tau_{lab}) = \frac{I_0}{4\pi^2} e^{-T_e} \left| \sum_{n=-\infty}^{\infty} J_n(p) e^{in\vartheta_0} \int_{-\infty}^{\infty} \frac{\exp\{-g(\omega)L - i\omega\tau_{lab}\}}{-i(\omega + n\Omega) + \Gamma_s/2} d\omega \right|^2, \quad (18)$$

where  $I_0 = \frac{cE_0^2}{8\pi}$  is the peak intensity of the field of incident photon (5a)-(5d) before transformation in the medium, and  $T_e = 2\delta_e L$  is the exponent factor of photoelectric absorption. Thus, in the case under consideration, the optical depth of the resonant absorber at frequency  $\omega$  is the sum of the resonant attenuation factor,  $\text{Re}\{g(\omega)L\}$ , specific for each frequency constituent, and the factor of photoelectric absorption,  $T_e$ , identical to all the constituents.

Let us note, that an intensity of the field of outgoing photon (the photon's waveform) in the laboratory reference frame (18) is the same as that in the reference frame of the oscillating absorber (see eq. (15) and Fig. 1b),  $I_{out}(\tau_{lab}) = I_{out}(\tau_a)$ , since  $|\exp\{\pm ip \sin(\Omega \tau_{lab} + \mathcal{G}_0) - i\Delta\varphi_0\}|^2 = 1$ . Using the vibrating reference frame allows one to considerably simplify the interpretation of changes in the photon waveform at the absorber exit.

### III. ANALYTICAL STUDY

As follows from (1), (15), and (18), propagation of photon through vibrating absorber results in transformation of the slowly-varying amplitude of the single-photon wave packet and the photon's waveform (Fig.1b, upper part). This transformation can be interpreted in different ways. In the laboratory reference frame, it results from coherent forward scattering of the photon by the resonant nuclei with absorption or emission of acoustic phonons having the frequency of vibration. In the reference frame of the oscillating absorber, as seen from (9) and (15), this transformation originates from temporal interference of the frequency constituents of multi-spike continuous spectrum of the transmitted field. Analysis of such an intricate interference can be simplified if the relation (15) is represented as a superposition of the exponentially decaying spectral components with carrier frequencies  $\omega_k = \omega_s + k\Omega$ , whose amplitudes acquire an additional temporal modulation owing to propagation through the resonant medium (Fig.1b, lower part),

$$\tilde{E}(L, \tau_a) = \theta(\tau_a) E_0 e^{i\varphi_0} e^{-T_e/2} e^{-\Gamma_s \tau_a/2} \sum_k A_k^{DB}(\tau_a) e^{-ik(\Omega \tau_a + \vartheta_0)}. \quad (19a)$$

where using solution from [23, 28], one can write the time-dependent term  $A_k^{DB}(\tau_a)$  of the  $k^{\text{th}}$  outgoing spectral component as,

$$A_k^{DB}(\tau_a) = J_{-k}(p) e^{-i\Delta\omega_k\tau_a} \sum_{n=0}^{\infty} \left( \frac{i\Delta\omega_k}{b} \right)^n (b\tau_a)^{\frac{n}{2}} J_n(2\sqrt{b\tau_a}), \quad (19b)$$

$\Delta\omega_k = \omega_a - \omega_s - k\Omega$ ,  $b = \gamma_a T_M / 2$ , and  $T_M = \frac{4\pi f_a n_{12} N |d_{12}|^2 \omega_a L}{\hbar c \sqrt{\epsilon} \gamma_a}$  is the Mössbauer thickness of

the absorber. The temporal modulation of the slowly-varying amplitude of an arbitrary  $k^{\text{th}}$  spectral component (19b) is the well-know dynamical beats [23, 24, 26, 29]. Its intensity,

$$I_k^{DB}(\tau_{lab}) = \theta(\tau_{lab}) I_0 e^{-T_e} e^{-\Gamma_s \tau_{lab}} J_{-k}^2(p) \left| \sum_{n=0}^{\infty} \left( \frac{i\Delta\omega_k}{b} \right)^n (b\tau_a)^{\frac{n}{2}} J_n(2\sqrt{b\tau_a}) \right|^2, \quad (19c)$$

was observed (in the case of absence of vibrations of both the source and absorber) for the first time in [23].

The dynamical beats of the  $k^{\text{th}}$  spectral component arise from selective interaction of its frequency constituents with the absorber transition. Since the bandwidth of the component is comparable to the linewidth of the resonant transition, it is not absorbed as a whole. Instead, its spectrum is altered due to different influence of the resonant absorption and resonant dispersion on its frequency constituents [23, 24, 26, 29]. Interference of the altered frequency constituents within the spectral contour results in dynamical beats of the  $k^{\text{th}}$  component. They become well visible if the bandwidth of the component is comparable to or larger than the linewidth of the resonant transition of an optically deep absorbing medium.

An alternative way to consider the output field in the vibrating reference frame (9), (15), (19a) is to represent it in the form of a superposition of the incident field and resonant-coherently-forward-scattered field. Using (5) one can rewrite the slowly-varying amplitude (15), (19a) as

$$\tilde{E}(L, \tau_a) = \theta(\tau_a) E_0 e^{i\varphi_0} e^{-T_e/2} e^{-\Gamma_s \tau_a/2} \sum_k \left\{ J_{-k}(p) + A_k^{FS}(\tau_a) \right\} e^{-ik(\Omega\tau_a + \vartheta_0)}. \quad (19d)$$

Here the first term in curly brackets is the exponentially decaying spectral component with carrier frequency  $\omega_k = \omega_s + k\Omega$  of the incident frequency-modulated field (5c) (with accounting for the global photoelectric absorption) and the second term is the resonant-coherently-forward-scattered field at the corresponding frequency. Comparing (19a) and (19d) one can write the time-dependent term  $A_k^{FS}(\tau_a)$  of the  $k^{\text{th}}$  forward-scattered-field component as

$$A_k^{FS}(\tau_a) = A_k^{DB}(\tau_a) - J_{-k}(p) = J_{-k}(p) \left\{ e^{-i\Delta\omega_k\tau_a} \sum_{n=0}^{\infty} \left( \frac{i\Delta\omega_k}{b} \right)^n (b\tau_a)^{\frac{n}{2}} J_n(2\sqrt{b\tau_a}) - 1 \right\}, \quad (19e)$$

Similar to dynamical beats, the  $k^{\text{th}}$  spectral component of the resonant-forward-scattered field has the amplitude modulation caused by the temporal interference of its spectral constituents within the spectral profile.

The interference of frequency constituents within each spectral component (19c) or (19e) of the superposition (19a) or (19d) is accompanied by the temporal interference between the spectral components as a whole. In other words, the dynamical beats (19b) interfere with each other, while the coherently-scattered-field components (19e) interfere both with each other and with the incident frequency-modulated field (4), (5). Let us consider this interference in more detail in the case where the oscillation frequency is much larger than linewidths of the source

and absorber,  $\Omega \gg \Gamma_s, 2\gamma_a$  and the central frequency of some  $m^{\text{th}}$  spectral component of the incident field in the oscillating reference frame (5a)-(5d),  $\omega_m = \omega_s + m\Omega$  (where  $m$  is an integer number), is resonant to the frequency  $\omega_a$  of transition  $|1\rangle \leftrightarrow |2\rangle$  of the absorber,  $\Delta\omega_m = 0$ . Then similar to [20] one can assume that only the resonant  $m^{\text{th}}$  spectral component interacts with this transition, while the other spectral components experience only the nonresonant photoelectric absorption. In such a case one has  $A_k^{DB}(\tau_a) = J_{-k}(p)$  and  $A_k^{FS}(\tau_a) = 0$  for  $k \neq m$ , while  $A_m^{DB}(\tau_a) = J_{-m}(p)J_0(2\sqrt{b\tau_a})$  and  $A_m^{FS}(\tau_a) = J_{-m}(p)\{J_0(2\sqrt{b\tau_a}) - 1\}$ . Thus the slowly varying amplitude of the output field in the oscillating reference frame (15) has a form of a superposition of the off-resonant spectral components transmitted without resonant interaction, and the  $m^{\text{th}}$  component, whose amplitude constitutes the dynamical beats:

$$\tilde{E}(L, \tau_a) = \theta(\tau_a) E_0 e^{i\phi_0} e^{-T_e/2} e^{-\Gamma_s \tau_a/2} \left\{ A^{pulse}(\tau_a) + A_m^{DB}(\tau_a) e^{-im(\Omega\tau_a + \mathcal{G}_0)} \right\}, \quad (20a)$$

$$A^{pulse}(\tau_a) = \sum_{n \neq -m} J_n(p) e^{in(\Omega\tau_a + \mathcal{G}_0)} = e^{ip \sin(\Omega\tau_a + \mathcal{G}_0)} - J_{-m}(p) e^{-im(\Omega\tau_a + \mathcal{G}_0)}, \quad (20b)$$

$$A_m^{DB}(\tau_a) = J_{-m}(p) J_0(2\sqrt{b\tau_a}), \quad (20c)$$

According to (20), the time dependence of intensity of the output radiation (18) can be now expressed in the following form,

$$I_{out}(\tau_{lab}) = \theta(\tau_{lab}) I_0 e^{-T_e} e^{-\Gamma_s \tau_{lab}} \left\{ |A^{pulse}|^2 + |A_m^{DB}|^2 + 2 \operatorname{Re} \left( A^{pulse} A_m^{DB} e^{im(\Omega\tau_a + \mathcal{G}_0)} \right) \right\} \quad (21a)$$

where

$$|A^{pulse}|^2 = 1 + J_{-m}^2(p) - 2J_{-m}(p) \cos[p \sin(\Omega\tau_{lab} + \mathcal{G}_0) + m(\Omega\tau_{lab} + \mathcal{G}_0)], \quad (21b)$$

$$|A_m^{DB}|^2 = J_{-m}^2(p) J_0^2(2\sqrt{b\tau_{lab}}), \quad (21c)$$

$$\begin{aligned} & 2 \operatorname{Re} \left( A^{pulse} A_m^{DB} e^{im(\Omega\tau_a + \mathcal{G}_0)} \right) \\ &= 2J_{-m} J_0(2\sqrt{b\tau_{lab}}) \left\{ \cos[p \sin(\Omega\tau_{lab} + \mathcal{G}_0) + m(\Omega\tau_{lab} + \mathcal{G}_0)] - J_{-m} \right\} \end{aligned} \quad (21d)$$

Equations (21) can be written in the equivalent compact form

$$\begin{aligned} I_{out}(\tau_{lab}) = \theta(\tau_{lab}) I_0 e^{-T_e} e^{-\Gamma_s \tau_{lab}} & \left\{ 1 + J_{-m}^2(p) \left[ J_0(2\sqrt{b\tau_{lab}}) - 1 \right]^2 + \right. \\ & \left. 2J_{-m}(p) \left[ J_0(2\sqrt{b\tau_{lab}}) - 1 \right] \cos[p \sin(\Omega\tau_{lab} + \mathcal{G}_0) + m(\Omega\tau_{lab} + \mathcal{G}_0)] \right\}, \end{aligned} \quad (21e)$$

which coincides with the result of [20].

As follows from Eqs. (20)-(21), both the slowly-varying amplitude of the single-photon wave packet,  $\tilde{E}(L, \tau_a)$ , and the waveform of the photon,  $I_{out}(\tau_{lab})$ , transmitted through an optically deep vibrating absorber, acquires two types of amplitude modulation. The first type is described by formulae (20b), (21b). It contributes into the total photon detection probability (21a) via relation (21b). This modulation is due to the absorber's vibration and was discussed in detail in [21]. Its origin can be explained as follows. At the entrance to the medium the spectrum of the photon (5a)-(5d) in the vibration reference frame constitutes a set of approximately  $2p+1$  equidistant spectral components separated by the frequency of oscillations. The amplitude of the  $n^{\text{th}}$

component is determined by Bessel function  $J_{-n}(p)$  of order  $-n$ . The central phase of the  $n^{\text{th}}$  component is determined by a sign of the corresponding Bessel function, as well as by the phase term  $n\mathcal{G}_0 - \varphi_0$ . Due to self-consistency of the incident spectrum, represented by the relation  $J_{-n}(p) = (-1)^n J_n(p)$ , the incident field (5) is frequency-modulated and does not have any amplitude modulation apart from the exponential factor  $\exp\{-\Gamma_s \tau_a/2\}$ . Elimination of the resonant  $m^{\text{th}}$  component as a whole, assumed in (20b), destroys the balance between the spectral components in the superposition. This results in appearance of amplitude modulation, which allows producing a train of short pulses under certain conditions [19-21]. Below just such conditions providing formation of pulses are considered and hence this off-resonant part of the incident field is marked by a superscript ‘‘pulse’’.

However, as discussed above, the resonant  $m^{\text{th}}$  spectral component is not eliminated as a whole but comes out of the absorber being reduced and spectrally transformed. In time domain its amplitude constitutes the dynamical beats described by the second term in (20a) (Fig.1b, green curve). So, both the slowly-varying amplitude of the single-photon wave packet (20a) and the waveform of the photon (21a), (21e) are shaped also owing to dynamical beats of the resonant  $m^{\text{th}}$  sideband described by formulae (20c), (21c). According to (21a), (21c), the waveform of dynamical beats of the resonant  $m^{\text{th}}$  sideband can be written as

$$I_m^{DB}(\tau_{lab}) = \theta(\tau_{lab}) I_0 e^{-T_e} e^{-\Gamma_s \tau_{lab}} J_{-m}^2(p) J_0^2\left(2\sqrt{b\tau_{lab}}\right). \quad (22)$$

As follows from (22), the waveform of dynamical beats of the  $m^{\text{th}}$  sideband constitutes a sequence of dips and humps in the time-dependent detection probability,  $I_m(\tau_{lab})$ . Timing of dips and humps of the dynamical beats is determined by zeros and extrema of Bessel function  $J_0\left(2\sqrt{b\tau_{lab}}\right)$ , where  $b = \gamma_a T_M/2$ , and thus by Mössbauer thickness of the absorber. In the case of a small Mössbauer thickness, the first dip and hump are situated far on the tail of the waveform of the transmitted photon and are negligible. With increasing value of the Mössbauer thickness the dips and humps are shifted towards the front of the waveform and become well visible.

The third term in (21a) represented by relation (21d) is due to interference of the dynamical beats with an amplitude modulation (pulses) caused by an absorber's vibration. This interference may be constructive or destructive subject to the phase relation between the fields constituting pulse(s) and dynamical beats at the exit from the absorber. This interference leads to increase or decrease of the pulse height. Timing of dynamical beats with respect to the front of the waveform is governed by Mössbauer thickness of the absorber,  $T_M$ , while position of the pulses produced via absorber's vibration is determined by the initial phase of vibration,  $\mathcal{G}_0$ . Therefore, the maximum amplitude of pulses can be achieved via the joint optimization of the parameters  $T_M$  and  $\mathcal{G}_0$  as follows from the formulas for the interference term in (21d,e). In the next section the optimization problem is studied analytically and numerically.

#### IV. OPTIMIZATION OF $\gamma$ -RAY PULSE FORMATION VIA RESONANT SUPPRESSION OF THE PHASE- MISALIGNED SIDEBAND

Maximization of a pulse amplitude and minimization of pulse duration implies finding the optimal values of the following parameters:  $\omega_a - \omega_s$ ,  $p$ ,  $T_M$ ,  $\mathcal{G}_0$ ,  $T_e$ ,  $\Omega$ . As shown in [20, 21], the quasi-monochromatic photon field can be transformed into a regular train of pulses subject to  $\omega_a - \omega_s = \pm\Omega$ , i.e., via suppression of the  $\pm 1^{\text{st}}$  ( $m = \pm 1$ ) sideband of the photon field in the oscillating reference frame by tuning it to the absorber resonance (choosing  $\Delta\omega_{-1} = 0$ ). It was shown also that maximizing amplitude of pulses is achieved in the case of maximization of the deleted sideband implemented at  $p^{\text{opt}} \approx 1.84$ . These conditions have clear interpretation in the vibrating reference frame. In this case, the field of the incident photon consists of five spectral components with considerably nonzero amplitudes, namely, the  $-2^{\text{nd}}$ ,  $-1^{\text{st}}$ ,  $0^{\text{th}}$ ,  $1^{\text{st}}$ , and  $2^{\text{nd}}$  component (Fig.1b, Fig.2). In the case of  $\mathcal{G}_0 = 0$ , and  $\varphi_0 = 0$ , considered in Fig. 2, the central phases (the initial phases at the central frequencies) of the  $0^{\text{th}}$ ,  $-1^{\text{st}}$ , and  $-2^{\text{nd}}$  components equal zero, while the central phases of the  $1^{\text{st}}$  and  $2^{\text{nd}}$  sidebands equal  $\pi$  and  $2\pi$ , respectively. Thus, the central phases of the  $-2^{\text{nd}}$ ,  $-1^{\text{st}}$ ,  $0^{\text{th}}$ , and  $2^{\text{nd}}$  (phase  $2\pi$  is equivalent to phase 0) spectral components are aligned along the horizontal line, while the central phases of the  $2^{\text{nd}}$ ,  $1^{\text{st}}$ ,  $0^{\text{th}}$ , and  $-2^{\text{nd}}$  (phase 0 is equivalent to phase  $-2\pi$ ) spectral components are aligned along the inclined (diagonal) line. Such a phase alignment holds also in the case  $\mathcal{G}_0 \neq 0$  and  $\varphi_0 \neq 0$  (when the  $n^{\text{th}}$  spectral component acquires an additional phase shift  $n\mathcal{G}_0 + \varphi_0$ ). However, a nonzero value of  $\mathcal{G}_0$  changes the slope of the lines, while a nonzero value of  $\varphi_0$  shifts the lines as a whole in vertical direction. Such a phase matching and specific amplitudes of the spectral components, proportional to  $|J_n(p)|$ , results in the absence of amplitude modulation of the incident photon field (4), (5), apart from the exponential decay  $\exp\{-\Gamma_s \tau_a / 2\}$ . Deletion of either the  $1^{\text{st}}$  or  $-1^{\text{st}}$  sideband (assuming elimination of the sideband as a whole) via tuning it to the absorber resonance (by a proper choice of constant velocity  $V_s$  (Fig.1b) of the source versus the absorber) destroys this balance and allows keeping only the phase-aligned components, whose interference in time domain leads to formation of a pulse train. If incomplete resonant absorption of the sideband is taken into account then the produced pulses interfere with the corresponding dynamical beats. As follows from Eqs. (20), (21), transition from deletion of the  $1^{\text{st}}$  sideband to deletion of the  $-1^{\text{st}}$  sideband shifts the pulses with respect to the front of the waveform by a half-cycle of absorber's vibration. So, for definiteness we shall consider the case of absorber resonance with the  $-1^{\text{st}}$  sideband.

Optimal value of the modulation index can be explained in terms of the coherent-forward-scattered field. According to (19d,e) a resonant interaction of the  $-1^{\text{st}}$  sideband with absorber leads to the output field amplitude in the form  $\tilde{E}(L, \tau_a) \propto e^{ip \sin(\Omega \tau_a + \vartheta_0)} + A_{-1}^{\text{FS}}(\tau_a) e^{i(\Omega \tau_a + \vartheta_0)}$ , where the first term represents the incident frequency-modulated field (4), (5) and  $A_{-1}^{\text{FS}}(\tau_a) = -J_1(p) \left\{ 1 - J_0(2\sqrt{b\tau_a}) \right\}$  is proportional to the amplitude of appeared forward-scattered field. The forward-scattered field is fully coherent with the resonant  $-1^{\text{st}}$  sideband and has the same carrier frequency. Temporal constructive interference of the forward-scattered field with the incident field leads to formation of pulses. The maximal pulse amplitude can be achieved subject to maximal value of  $A_{-1}^{\text{FS}}(\tau_a)$  which corresponds to maximization of  $J_1(p)$  implemented at  $p = p^{\text{opt}}$  where  $J_1(p)$  is the normalized amplitude of the  $-1^{\text{st}}$  spectral sideband.

Hence, maximizing the amplitude of the resonant 1<sup>st</sup> or -1<sup>st</sup> sideband of the incident field is the necessary condition for obtaining the highest pulse amplitude.

Let us find the values of  $T_M$  and  $\mathcal{G}_0$ , maximizing the peak intensity of the produced pulses in case, where the modulation index is  $p^{opt}$  and absorber is tuned to the resonance with the -1<sup>st</sup> sideband,  $\Delta\omega_{-1} = 0$ . First, let us consider the finite values of  $T_M$  and a small value of the ratio  $\gamma_a/\Omega \ll 1$ , such that only the resonant -1<sup>st</sup> sideband interacts with the absorber transition and the analytical results (20)-(22) are valid. The output photon waveform (21) is locally maximized (for arbitrary value of  $p$ ), if  $\cos[p \sin(\Omega\tau_{lab} + \mathcal{G}_0) + m(\Omega\tau_{lab} + \mathcal{G}_0)] = -1$ . For  $m = -1$  this corresponds to  $p \sin(\Omega\tau_{lab} + \mathcal{G}_0) - \Omega\tau_{lab} - \mathcal{G}_0 = (2k + 1)\pi$  and hence

$$\Omega\tau_{lab} + \mathcal{G}_0 = (2k + 1)\pi, \quad (23a)$$

where  $k$  is an integer number labeling the modulation peaks. Under the condition (23a), equations (21) can be written in the form

$$I_{out}^{peak}(\tau_{lab}) = I_0 F_1(\tau_{lab}) F_2(\tau_{lab}) \quad (23b)$$

were

$$F_1(\tau_{lab}) = \theta(\tau_{lab}) e^{-T_e} e^{-\Gamma_s \tau_{lab}}, \quad (23c)$$

$$\begin{aligned} F_2(\tau_{lab}) &= |A_{\max}^{pulse}|^2 + |A_{-1}^{DB}|^2 + 2 \operatorname{Re} \left( A_{\max}^{pulse} A_{-1}^{DB} e^{-i(\Omega\tau_a + \mathcal{G}_0)} \right) \\ &= \left\{ 1 + J_1(p) \left[ 1 - J_0 \left( 2\sqrt{b\tau_{lab}} \right) \right] \right\}^2 \end{aligned} \quad (23d)$$

It follows from (21) that

$$|A_{\max}^{pulse}|^2 = [1 + J_1(p)]^2, \quad (24a)$$

$$|A_{-1}^{DB}|^2 = J_1^2(p) J_0^2 \left( 2\sqrt{b\tau_{lab}} \right), \quad (24b)$$

$$2 \operatorname{Re} \left( A_{\max}^{pulse} A_{-1}^{DB} e^{-i(\Omega\tau_a + \mathcal{G}_0)} \right) = -2J_1(p) J_0 \left( 2\sqrt{b\tau_{lab}} \right) [1 + J_1(p)]. \quad (24c)$$

At  $p = p^{opt}$  local maxima are peaks of pulses, so that equations (23) and (24) describe the time dependence of the peak intensity of the pulses. The function  $F_1(\tau_{lab})$  is the waveform of the incident photon attenuated as a whole by the photoelectric absorption only. It has maximum,  $F_1^{\max} = 1$ , at  $T_e = 0$  and  $\tau_{lab} = 0$ . The function  $F_2(\tau_{lab})$  determines the value of pulse peaks over  $F_1(\tau_{lab})$  accounting for interference of pulses due to vibration with dynamical beats of the -1<sup>st</sup> component. As follows from (23d) and (24), if interference is absent or negligible ( $J_0(2\sqrt{b\tau_{lab}}) = 0$  or  $J_0(2\sqrt{b\tau_{lab}}) \ll 1$  occurred in deeps of dynamical beats or if  $b\tau_{lab} \gg 1$ , respectively), then  $F_2(\tau_{lab}) \approx 2.5$ . The function  $F_2(\tau_{lab})$  takes the maximum value,  $F_2(\tau_{lab}) = F_2^{\max} \approx 3.3$ , when the minimum of  $J_0(2\sqrt{b\tau_{lab}}) \approx -0.4$  is achieved at  $2\sqrt{b\tau_{lab}} \approx 3.8$ . This occurs at the first hump of dynamical beats (21c), (22), (24b) resulting in a maximum constructive interference between the pulses (20b) and dynamical beats (20c). Maximization of the interference term (24c) gives the largest enhancement in pulse amplitude,  $2 \operatorname{Re} \left( A_{\max}^{pulse} A_{-1}^{DB} e^{-i(\Omega\tau_a + \mathcal{G}_0)} \right)_{\max} \approx 0.7$ . On the other hand, if some pulse peak coincides with the second hump of dynamical beats (21c), (22), (24b) corresponding to the first local maximum of

$J_0(2\sqrt{b\tau_{lab}}) \approx 0.3$ , achieved at  $2\sqrt{b\tau_{lab}} \approx 7$ , the maximum destructive interference (minimum value of the interference term (24c),  $2 \operatorname{Re}\left(A_{\max}^{pulse} A_{-1}^{DB} e^{-i(\Omega\tau_a + \vartheta_0)}\right)_{\min} \approx -0.6$ ) between the pulses (20b) and dynamical beats (20c), occurs. In this case dynamical beats reduce the pulse amplitude resulting in  $F_2(\tau_{lab}) = F_2^{\min} \approx 1.98$ .

In order to maximize the product  $F_1(\tau_{lab})F_2(\tau_{lab})$  one should simultaneously maximize Mössbauer thickness (in order to reduce  $\tau_{lab}$  in the exponent  $e^{-\Gamma_s\tau_{lab}}$  keeping unchanged the optimal value of  $2\sqrt{b\tau_{lab}} = \sqrt{2\gamma_a T_M \tau_{lab}}$ ) and minimize  $T_e$ . However,  $T_e$  is proportional to  $T_M$  and is ultimately determined by the percentage of the resonant nuclei: the higher percentage of the resonant nuclei, the smaller physical thickness  $L$  of the absorber and, hence, the smaller photoelectric attenuation. Hence minimization of  $T_e$  can be done via enrichment of the absorber with the resonant nuclei. Similar to [19], we assume that  $^{57}\text{Fe}$  nuclei are embedded into stainless steel which is a compound Fe:Cr:Ni at 70:19:11 wt%. However, unlike [19] where the natural abundance  $\sim 2.2\%$  of  $^{57}\text{Fe}$  in iron fraction was used, in order to minimize  $T_e$ , we assume the commercially available 90% enrichment of iron fraction by nuclide  $^{57}\text{Fe}$  with natural broadening of spectral line of the resonant transition, implying  $\gamma_a = \Gamma_s/2$  and  $2\sqrt{b\tau_{lab}} = \sqrt{T_M \Gamma_s \tau_{lab}}$ . Taking into account that the photoelectric absorption coefficient in stainless steel is  $2\delta_e \approx 5.06 \div 5.17 \times 10^4 \text{ m}^{-1}$  [30], we get  $T_e \approx T_M/180$ . Let us maximize Eq. (23b) for the above parameters values. Finding the partial derivatives of  $I_{out}^{peak}$  over  $\tau_{lab}$  and  $T_M$ , and equating them to zero after some transformations we get:

$$J_1(p^{opt}) \frac{J_1(\sqrt{T_M \Gamma_s \tau_{lab}})}{\sqrt{T_M \Gamma_s \tau_{lab}}} = \frac{1}{T_M} \left\{ 1 + J_1(p^{opt}) \left[ 1 - J_0(\sqrt{T_M \Gamma_s \tau_{lab}}) \right] \right\}, \quad (25a)$$

$$\left\{ 1 + J_1(p^{opt}) \left[ 1 - J_0(\sqrt{T_M \Gamma_s \tau_{lab}}) \right] \right\} (\Gamma_s \tau_{lab} - T_M/180) = 0 \quad (25b)$$

Eq. (25b) has a solution  $T_M = 180\Gamma_s \tau_{lab}$ . Substituting it into Eq. (25a) we find

$$J_0(13.42\Gamma_s \tau_{lab}) + 13.42J_1(13.42\Gamma_s \tau_{lab}) - 2.719 = 0 \quad (25c)$$

The roots of this equation are  $\Gamma_s \tau_{lab} \approx [0.02; 0.24; 0.58; 0.69; 1.08; 1.12]$ . The respective values of absorber Mössbauer thickness are  $T_M \approx [3.5; 44; 103.6; 123.8; 195.1; 201.6]$ . According to (23), these values of  $\Gamma_s \tau_{lab}$  and  $T_M$  correspond to the following values of the peak pulse intensity:  $I_{out}^{peak}/I_0 \approx [0.98; 1.94; 0.66; 0.70; 0.27; 0.27]$ . Thus, the largest maximum,  $\operatorname{Max}\{I_{out}^{peak}/I_0\} \approx 1.94$  of pulse height is achieved at  $\Gamma_s \tau_{lab}^{opt} \approx 0.24$  and  $T_M^{opt} \approx 44$ , corresponding to the physical thickness of the film  $L \approx 4.8 \mu\text{m}$ . The respective optimal values of the initial phase of vibration are  $\vartheta_0^{opt} \approx (2k+1)\pi - 0.24\Omega/\Gamma_s$ . The waveform corresponding to these optimal parameter values is plotted in Fig.3 for  $\gamma_a/\Omega \approx 5.8 \times 10^{-4}$ . In this case, according to (23c), one has  $F_1(\tau_{lab}) = 0.78\theta(\tau_{lab})e^{-\Gamma_s\tau_{lab}}$ , where  $\theta(\tau_{lab})e^{-\Gamma_s\tau_{lab}}$  is the waveform of the incident photon represented by black dashed curve in Fig.3. It can be seen that because of the exponential dependence of  $F_1(\tau_{lab})$ , the value  $\operatorname{Max}\{I_{out}^{peak}/I_0\} \approx 1.94$  is achieved slightly earlier, at

$2\sqrt{b\tau_{lab}} \cong 3.3$ , than the first hump of dynamical beats, occurred at  $2\sqrt{b\tau_{lab}} \cong 3.8$ . For  $T_M^{opt} \approx 44$  the respective times are  $\tau_{lab} \approx 35ns$  for maximum of pulse height, and  $\tau_{lab} \approx 46ns$  for the first hump of dynamical beats.

The accuracy of obtained analytical results decreases with increasing value of  $\gamma_a/\Omega$ . This is because the other spectral components of the photon field are also influenced by the resonant absorption and primarily by the resonant dispersion, which lead to (i) change of central phases of the spectral components and (ii) distortion of amplitudes and primarily phases of Fourier constituents within the spectral contour of each component. As a result, the exact solution for the waveform of the output photon (18) and the corresponding optimal values of  $\Gamma_s\tau_{lab}$  and  $T_M$  deviate from the results of the analytical study.

Let us trace the dependence of these deviations as a function of the frequency of absorber's vibration. In Figs 4a,b we show the optimal values of (a) Mössbauer thickness,  $T_M^{opt}(\Omega)$ , and (b) the moment of formation of pulse with the highest intensity,  $\tau_{lab}^{opt}(\Omega)$ , found via the numerical analysis of Eq. (18), versus the frequency of vibration. Figure 4c shows the frequency dependence of maximum intensity of the highest pulse (maximum of the peak detection probability),  $\text{Max}\{I(\tau_{lab})/I_0\} = I_{out}^{peak}(T_M^{opt}(\Omega), \tau_{lab}^{opt}(\Omega), \mathcal{G}_0^{opt}(\Omega))/I_0 = I_{max}(\Omega)/I_0$ . In all the Figs. 4a-c the numerical results are compared with the analytical solution. As can be seen, at high frequencies of vibration,  $\Omega/(2\pi) > 150\text{MHz}$ , the results of numerical optimization and the analytical solution almost coincide. This means that maximum of the peak detection probability practically does not depend on the vibration frequency and is  $I_{max}/I_0 \approx 1.94$  as has been found within the analytical model. This value is achieved at  $\tau_{lab}^{opt} \approx 35ns$  and can be implemented with an absorber of Mössbauer thickness  $T_M^{opt} \approx 44$  irrespective of the vibration frequency. This is because at such vibration frequencies and Mössbauer thickness only the  $-1^{st}$  spectral component of the photon field is really altered during propagation through the absorber. As shown in [19], the pulse repetition rate equals the vibration frequency and pulse duration is defined by inverse of the product of phase-aligned components and the vibration frequency. Therefore the shortest pulse duration that could be produced by the discussed technique is limited by the highest available vibration frequency of piezo-transducer with the desired amplitude and linewidth. The maximum frequency of the diamond piezoelectric transducer is 970 MHz [31]. In this case the regular pulse sequence shown in Fig. 3 can be produced with pulse duration of about 190 ps. The polyvinylidene fluoride (PVDF) piezo-electric transducers operating at frequencies up to 24 GHz [32] allows producing pulses to 7.7 ps.

At frequencies below 150 MHz the discrepancy between the analytical and numerical results increases as the frequency decreases, reaching maximum at the lowest considered vibration frequency (Fig.4). This is caused by increasing influence of nuclear transition on the off-resonant spectral components of the photon field. At the considered vibration frequencies  $\Omega/\Gamma_s \geq 10$  one can neglect the resonant absorption of the off-resonant spectral components. However, the resonant dispersion can noticeably modify the phase relations both between the frequency constituents within each off-resonant spectral component and between central phases of spectral components owing to their different phase incursion during propagation through the medium. According to (13b), (14), the phase incursion of an arbitrary spectral constituent of the photon field with

frequency  $\omega$  at the absorber exit is  $\Phi(\omega)=\text{Im}\{g(\omega)L\}=\frac{T_M\gamma_a}{2}\frac{(\omega_a-\omega_s-\omega)}{\gamma_a^2+(\omega_a-\omega_s-\omega)^2}$ . This means that,

for instance, the phase misalignment at carrier frequencies of the closest to nuclear transition -2<sup>nd</sup> and 0<sup>th</sup> components behind the absorber is  $\Delta\Phi_{-2,0}=\Phi(-2\Omega)-\Phi(0)=\Gamma_s T_M/(2\Omega)$ . At

$\Gamma_s/(2\pi)=1\text{MHz}$ ,  $\Omega/(2\pi)=10\text{MHz}$ , and  $T_M^{opt}=20$  (the first circle in Fig. 4a-c) the phase misalignment is  $\Delta\Phi_{-2,0}\approx\pi/3$ . Such phase distortions noticeably change the temporal interference pattern, optimal values of  $T_M^{opt}$ ,  $\mathcal{G}_0^{opt}$ , and  $\tau_{lab}^{opt}$ , as well as the highest peak pulse intensity  $I_{max}/I_0$  (Fig.4, difference in pulse shape is well-visible in Figures 3,7,8). The changes in the temporal interference pattern are taken into account in relations (19), (20). They can be interpreted via generation of the off-resonant spectral components of the forward-scattered field with time-dependent amplitudes (19d), and the temporal interference of the forward-scattered-field components with both pulses and dynamical beats of the -1<sup>st</sup> spectral component (20) as following

$$\tilde{E}(L,\tau_a)=\theta(\tau_a)E_0e^{i\varphi_0}e^{-T_e/2}e^{-\Gamma_s\tau_a/2}\left\{A^{pulse}(\tau_a)+A_{-1}^{DB}(\tau_a)e^{-i(\Omega\tau_a+\mathcal{G}_0)}+\sum_{k\neq-1}A_k^{FS}(\tau_a)e^{-ik(\Omega\tau_a+\mathcal{G}_0)}\right\}. \quad (26)$$

As shown in Fig. 4, for every vibration frequency there is some optimal Mössbauer thickness,  $T_M^{opt}$ , and initial vibration phase,  $\mathcal{G}_0^{opt}$ , at which the constructive interference of the terms in (26) results in the highest peak pulse intensity  $I_{max}/I_0$  at the corresponding moment  $\tau_{lab}^{opt}$ . At vibration frequencies  $\Omega/(2\pi)<18\text{MHz}$  large distortions of the output spectral components, caused by off-resonant forward-scattered field, hamper pulse formation via resonant absorption of the -1<sup>st</sup> component [ $I_{max}/I_0$  is less than that followed from the analytical model neglecting the off-resonant forward-scattered field (Fig. 4c)]. As the vibration frequency growth, the phase misalignment at optimal conditions becomes smaller in spite of increasing optimal Mössbauer thickness (for example, at  $\Omega/(2\pi)=30\text{MHz}$  and  $T_M^{opt}=40$  the phase misalignment is  $\Delta\Phi_{-2,0}\approx\pi/5$ ). Moreover, at  $\Omega/(2\pi)>18\text{MHz}$  contribution of the off-resonant forward-scattered field at the moment  $\tau_{lab}^{opt}$  becomes constructive leading to enhancement in peak pulse intensity [ $I_{max}/I_0$  becomes larger than that followed from the analytical model (Fig. 4c)]. At vibration frequency  $\Omega/(2\pi)\approx 30\text{MHz}$  the constructive interference of all the transmitted frequency constituents (of all the terms in (26)) results in a global maximum of photon peak detection probability,  $I_{max}^{Glob}/I_0\approx 2.02$ , that occurs at  $\tau_{opt}^{Glob}\approx 28\text{ns}$  and  $\mathcal{G}_0^{Glob}\approx 5\pi/4$  upon  $T_M^{Glob}\approx 40$ . It should be mentioned that the optimal quite high Mössbauer thickness,  $T_M^{Glob}\approx 40$  is experimentally feasible since it corresponds to the physical thickness of the stainless steel film  $L\approx 4.4\mu\text{m}$ . This global maximum is shown in Fig.5a by gray spot at the coordinate plane of the Mössbauer thickness,  $T_M$ , and the initial phase of absorber's vibration,  $\mathcal{G}_0$ . As can be seen, deviation of either  $T_M$  or  $\mathcal{G}_0$  from their optimal values results in decrease of the peak detection probability,  $I_{out}^{peak}(T_M,\tau_{lab}^*,\mathcal{G}_0)<I_{max}^{Glob}/I_0$  (where  $\tau_{lab}^*\equiv\tau_{lab}(T_M,\mathcal{G}_0)$  corresponds to the top of the highest pulse) because of violation of the constructive interference condition.

A peak detection probability qualitatively similar to the one displayed in Fig.5a could be plotted also in the above discussed case of high vibration frequency,  $\Omega/(2\pi)>150\text{MHz}$ , where contribution of the phase distortion is negligible, while the constructive interference between the

pulses due to vibration and dynamical beats of the  $-1^{\text{st}}$  spectral component would provide the largest value of  $I_{out}^{peak}(T_M, \tau_{lab}^*, \mathcal{G}_0)$  at  $T_M \rightarrow \infty$  and  $\tau_{lab}^* \rightarrow 0$ . This is because at  $T_M < T_M^{opt}$  the insufficiently attenuated resonant  $-1^{\text{st}}$  sideband of the photon field spoils the pulse formation. At  $T_M > T_M^{opt}$  the  $-1^{\text{st}}$  sideband is attenuated stronger. As a result, constructive interference of the remaining in-phase components leads to formation of the pulses with higher amplitude. However, with increasing  $T_M$  the nonresonant photoelectric absorption coefficient  $T_e$  also grows (in the considered case  $T_e = T_M/180$ ), leading to attenuation of the photon field as a whole and reduction of the output photon detection probability. The photoelectric attenuation plays the major role in formation of maximum photon detection probability at relatively low percentage of the resonant nuclei, i.e., upon the condition  $\Gamma_s T_M / \Omega \ll T_e$ . Otherwise (including the case  $T_e = 0$ ) the above discussed interference can not be neglected.

The temporal interference plays the major role in formation of ‘‘jump’’ in dependences of  $T_M^{opt}(\Omega)$  and  $\tau_{lab}^{opt}(\Omega)$ , as well as a kink of function  $I_{max}(\Omega)/I_0$  at  $40 \text{ MHz} < \Omega/(2\pi) < 45 \text{ MHz}$  (Fig. 4). As can be seen from Fig. 4c, starting from frequency  $\Omega/(2\pi) \approx 35 \text{ MHz}$ , the temporal interference between the constituents of the outgoing field (26) is able to produce at the same vibration frequency  $\Omega$  two maxima,  $I_{max}/I_0$  (filled marks) and  $I'_{max}/I_0$  (open marks) in the peak detection probability of the output field achieved at the corresponding values  $T_M^{opt}$  and  $T'_M$  (filled and open marks, respectively, in Fig 4a) as well as  $\tau_{lab}^{opt}$  and  $\tau'_{lab}$  (filled and open marks, respectively, in Fig 4b). This is illustrated in Fig.5b for  $\Omega/(2\pi) \approx 45 \text{ MHz}$  by two grey spots situated at larger Mössbauer thickness (corresponding to earlier instant  $\tau'_{lab}$  (open blue circle) in Fig.4b) and at smaller Mössbauer thickness (corresponding to later instant  $\tau_{lab}^{opt}$  (filled red rhomb) in Fig.4b). At  $35 \text{ MHz} < \Omega/(2\pi) < 45 \text{ MHz}$  one has  $I_{max} > I'_{max}$  under  $T_M^{opt} > T'_M$  and  $\tau_{lab}^{opt} < \tau'_{lab}$  (filled circles and open rhombs in Fig. 4a-c, respectively). However, maximum peak detection probability decreases with increasing vibration frequency. At the same time, the second maximum in the peak detection probability, achieved at smaller Mössbauer thickness and later times (red open rhombs in Fig4), grows. Starting from vibration frequency  $\Omega/(2\pi) \approx 45 \text{ MHz}$ , smaller Mössbauer thickness and later moments provide larger value of peak detection probability and become optimal (open rhombs become filled rhombs). At frequencies  $\Omega/(2\pi) > 75 \text{ MHz}$  maximum in peak detection probability at high Mössbauer thickness and early times disappears. At the coordinate plane of the Mössbauer thickness,  $T_M$ , and the initial phase of absorber’s vibration,  $\mathcal{G}_0$ , the peak detection probability at this frequency range has a similar look with single grey spot as in the case  $\Omega/(2\pi) < 35 \text{ MHz}$  displayed in Fig.5a.

The spectrum of the output photon field in the oscillating reference frame under the most optimal conditions providing the highest peak detection probability,  $I_{max}^{Glob}/I_0 \approx 2.02$ , at  $\Omega/(2\pi) = 30 \text{ MHz}$ ,  $T_M^{Glob} = 40$ , and  $\mathcal{G}_0^{Glob} = 5\pi/4$ , is shown in Fig. 6. The  $-1^{\text{st}}$  sideband is almost fully absorbed (except for the spectral wings corresponding to dynamical beats in time representation), and only the phase-aligned  $-2^{\text{nd}}$ ,  $0^{\text{th}}$ ,  $1^{\text{st}}$  and  $2^{\text{nd}}$  spectral components remain. However, the spectral phase of the field (shown by red dashed curve) is noticeably distorted with respect to that in Fig. 2 due to interaction of nonresonant components with the absorber transition. The cen-

tral phases of the  $-2^{\text{nd}}$  and  $0^{\text{th}}$  components are shifted at  $\pm\pi/5$  from dashed green line. In the time domain interference of the remaining spectral components of the photon field leads to formation of the pulse train shown in Fig. 7 with the highest peak detection probability,  $I_{\text{max}}^{\text{Glob}}/I_0 \approx 2.02$ . For chosen vibration frequency the duration of the first pulse is about 6 ns. Black dash-dotted curve shows the waveform of the photon at the absorber entrance and clearly demonstrates that although the photon field undergoes both resonant and photoelectric absorption, the peak detection probability of the transmitted photon is more than two times higher, than the peak detection probability at the absorber entrance. Red dotted curve, plotted according to equation (23), traces the pulse height versus time,  $\tau_{\text{lab}}$ , at the same parameter values ( $p = p^{\text{opt}}$ ,  $T_M = T_M^{\text{Glob}}$ ) with accounting for the dynamical beats of the  $-1^{\text{st}}$  sideband only. Its maximum indicates the highest detection probability under that approximation. It can be seen that taking into account the off-resonant spectral components of the forward-scattered field and their temporal interference with both pulses due to vibration and dynamical beats of the  $-1^{\text{st}}$  component leads to increase in the highest detection probability and its shift towards photon's front edge.

The numerically plotted pulses [according to exact formula (18)], and the curve [plotted according to approximate formula (23)] roughly tracing their peaks (blue and red lines in Fig. 7) allow to track the periodic dependence of peak detection probability of the photon on the initial phase of absorber's vibration, shown in Fig. 5. In accordance with the analytical solution, the optimal value of the initial phase of vibration is  $\mathcal{G}_0^{\text{opt}} = (2k + 1)\pi - 0.24\Omega/\Gamma_s$  (where  $k$  is an integer number). At this value of  $\mathcal{G}_0$  the respective  $k^{\text{th}}$  pulse from the produced pulse train (21), centered at  $\tau_{\text{lab}} = ([2k + 1]\pi - \mathcal{G}_0^{\text{opt}})/\Omega$ , is tuned to maximum of the envelope (23). Deviation of the initial phase of vibration from its optimal value leads to a shift of the position of the  $k^{\text{th}}$  pulse from the maximum of the envelope, and reduction of its intensity. However, whether the  $k^{\text{th}}$  pulse is shifted to the right or to the left, a neighboring (either  $k - 1$  or  $k + 1$ ) pulse moves towards the peak of the envelope, and after a  $2\pi$  shift of the initial phase of vibration it occupies the optimal position.

In order to illustrate the effect of joint optimization of the absorber optical depth and the initial oscillation phase, in Fig. 8 we compare the optimized photon waveform, produced at the frequency of vibration  $\Omega/(2\pi) = 10.2\text{MHz}$ , to the waveform, plotted for the parameter values used in the experiment [19]. The photon waveform in the proof-of-principle experiment [19] (red dotted curve) was produced in a stainless steel film with natural abundance, 2.2%, of  $^{57}\text{Fe}$  in iron fraction. This resulted in strong photoelectric absorption,  $T_e \approx 1.27$ . As a result the peak pulse intensity was  $I_{\text{max}}(2\%)/I_0 \approx 0.3$ . The only enrichment of the stainless steel absorber by the resonant nuclei to 90% in iron fraction results in reduction of photoelectric absorption to  $T_e \approx 0.1$  and increasing the photon transmission as a whole. As a result, the peak pulse intensity also increases to  $I_{\text{max}}(90\%)/I_0 \approx 1.04$  (green dashed curve). Although the peak pulse intensity in this case only slightly exceeds the intensity at front of the incident photon, the enhancement in peak pulse intensity due to enrichment is about 3.5 times. However, the pulse contrast, defined as the difference between intensities at maximum and the left minimum, is only  $(I_{\text{max}}(90\%) - I_{\text{min}}(90\%))/I_0 \approx 0.55$ . Optimization of the absorber's Mössbauer thickness accounting for interference of pulses with dynamical beats and the off-resonant forward-scattered

field (blue solid curve), results in (i) enhancement in peak pulse intensity to  $I_{\max}^{opt}/I_0 \simeq 1.6$  and (ii) enhancement in the pulse contrast to  $(I_{\max}^{opt} - I_{\min}^{opt})/I_0 \simeq 1.6$ . Thus, the optimization allows producing the true pulses with maximum detection probability of the transformed photon considerably exceeding the maximum detection probability of the photon emitted by the source.

## V. $\gamma$ -RAY PULSE FORMATION VIA FLIP OF PHASE- MISALIGNED SIDEBAND

Up to now we considered the possibilities for transforming the waveform of the incident photon into the pulse train via suppression of the anti-phase (phase-misaligned) -1<sup>st</sup> sideband of the photon field by means of its resonant absorption. However, instead of suppression, this sideband can be made in-phase (phase-aligned) with respect to the other sidebands of the photon field via the resonant dispersion of the absorber. In order to do this, one needs to provide  $\pi$  phase-shift at the central frequency of the -1<sup>st</sup> sideband, which implies detuning of its central frequency from the frequency of the resonance by the value

$$\Delta\omega_{-1} = \omega_a - \omega_s + \Omega = \frac{T_M \gamma_a}{4\pi} + \gamma_a \sqrt{\left(\frac{T_M}{4\pi}\right)^2 - 1}. \quad (27)$$

Similarly to the case of absorption of the -1<sup>st</sup> sideband, studied above, we performed a numerical search for the optimal conditions, maximizing the output photon detection probability (18) after transmission through the resonant absorber, which provides  $\pi$  phase-shift of the -1<sup>st</sup> sideband of the photon field. At the frequency of vibration  $\Omega/2\pi = 40$  MHz the optimal parameters are  $T_M \simeq 50$ ,  $\mathcal{G}_0 \simeq 7\pi/6$ , and  $\Delta\omega_1/(2\pi) \simeq 4.4$  MHz. The corresponding waveform of the output photon is shown in Fig. 9 by red dashed line along with the optimized waveform for the case of suppression of the -1<sup>st</sup> sideband, plotted by black solid line. The spectrum of the output photon field in the vibrating reference frame in the case of  $\pi$  phase-shift of central frequency of the -1<sup>st</sup> sideband is shown in Fig. 10. One may expect that, since instead of deletion of the anti-phase sideband of the photon field it is tuned in-phase with the others, the peak detection probability of the output photon should increase. This is true starting from the third pulse in the train and for the overall detection probability of the output photon (the detection probability within a sufficiently long time-interval), as well as for the case of time-averaging of detection probability over the instants of formation of excited state of radiating nucleus [22]. At the same time, the highest detection probability, achieved at the peak of the first pulse, is larger in the case of suppression of the -1<sup>st</sup> sideband via the resonant absorption. In order to understand this, one needs to take into account the effect of group velocity dispersion on the field of the -1-st sideband. As follows from Eqs. (9), (13), and (14), the real part of wavenumber of the photon field strength in the vibrating reference frame is

$$k = \frac{\omega}{c} + \frac{T_M}{2L} \frac{\gamma_a (\omega_a - \omega)}{\gamma_a^2 + (\omega_a - \omega)^2}. \quad (28)$$

This leads to the expression for the group velocity,  $v_{gr} = d\omega/dk$ , in the form

$$\frac{1}{v_{gr}} = \frac{1}{c} + \frac{T_M \gamma_a}{2L} \frac{(\omega_a - \omega)^2 - \gamma_a^2}{\left[(\omega_a - \omega)^2 + \gamma_a^2\right]^2}. \quad (29)$$

Since the -1<sup>st</sup> sideband of the photon field is much closer to the resonance than the others, one may take into account the effect of the group velocity dispersion only on this sideband. Thus, for the -1<sup>st</sup> sideband one has  $\frac{1}{v_{gr}} = \frac{1}{c} + \frac{T_M \gamma_a}{2L} \frac{\Delta\omega_{-1}^2 - \gamma_a^2}{[\Delta\omega_{-1}^2 + \gamma_a^2]}$ , while for the other spectral components

one can assume  $\frac{1}{v_{gr}} \approx \frac{1}{c}$  (since in the considered case  $\Omega \approx 71\gamma_a$ ). This difference in group velocities leads to a delay of the field of the -1<sup>st</sup> sideband with respect to the others by the value  $\tau_d = \frac{T_M \gamma_a}{2} \frac{\Delta\omega_{-1}^2 - \gamma_a^2}{[\Delta\omega_{-1}^2 + \gamma_a^2]}$ . In the optimal case considered in Figs. 10 and 11 the delay is

$\tau_d = 110\text{ns}$ , which gives a good estimate for the moment of time, at which  $\pi$  phase-shift of the -1<sup>st</sup> sideband provides the biggest increase in the amplitude of the pulses, with respect to the case of suppression of this sideband, see Fig. 9. In a sufficiently thick absorber,  $T_M \gg 4\pi$ , the optimal value of detuning satisfies the relation  $\Delta\omega_{-1} \approx T_M \gamma_a / 2\pi$ , so that the group delay of the -1<sup>st</sup> sideband is  $\tau_d \approx 2\pi^2 / (T_M \gamma_a)$ . Thus, the delay of the -1<sup>st</sup> sideband decreases with increasing absorber thickness, as shown in Fig. 10, where we plot the analytically calculated envelopes of the pulses, produced from the waveform of the incident photon (i) via  $\pi$  phase-shift of the -1<sup>st</sup> sideband, Eqs. (18), (27), and (ii) via the resonant absorption of this sideband, Eq. (21). The calculations were done for  $T_M = 50, 100$ , and  $150$ , and optimal values of the other parameters. For all the considered values of Mössbauer thickness, the highest detection probability is achieved in the case of suppression of the -1<sup>st</sup> sideband via the resonant absorption. However, the resonant dispersion provides an additional tool for manipulation of the photon waveform and allows one to get higher average detection probability of the transmitted photon.

## VI. CONCLUSION

In this paper we discussed the ultimate capabilities for transformation of the exponentially decaying waveform of a Mössbauer 14.4 keV photon from  $^{57}\text{Co}$  radioactive source into a regular sequence of the shortest pulses with the highest temporal photon detection probability in an optically deep sinusoidally vibrating  $^{57}\text{Fe}$  recoilless resonant absorber. We showed that the shortest pulse duration that could be produced by the discussed technique is limited by the highest available vibration frequency of piezo-transducer and at present be as short as 7.7 ps. The highest temporal detection probability of the photon is determined by the optimal conditions (optical depth of the absorber, frequency and initial phase of its vibration) providing simultaneously (i) the largest amplitude of both incident and resonant-coherently-forward-scattered fields of the single-photon wave packet, and (ii) the constructive interference of these fields. In the case of stainless steel absorber with 90% enrichment by  $^{57}\text{Fe}$  nuclide in iron fraction, the highest achievable peak detection probability of photon at the exit from the absorber is shown to be about two times higher than the peak detection probability of photon emitted by the source. It is achieved under the experimentally feasible conditions with a stainless steel film of  $\approx 4.4\mu\text{m}$  physical length, vibrating with  $\approx 30\text{MHz}$  frequency.

Manipulating a single-photon waveform can be used for quantum information processing as well as for the development of a table-top single-photon source of hard x-ray / $\gamma$ -ray pulses for

the Mössbauer spectroscopy of various non-stationary processes with time resolution up to ten picoseconds.

## VI. AKNOWLEGMENTS

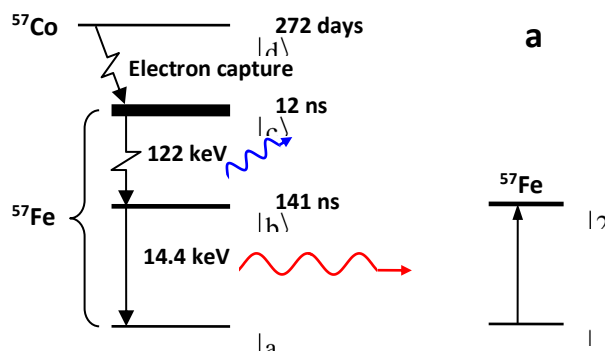
We acknowledge support by RFBR under the grants No. 16-32-60173, No. 16-02-01034, and No. 18-32-00774, as well as support by NSF under the grant No. PHY-150-64-67. The analytical studies presented in Sections II-IV were supported by the Ministry of Education and Science of the Russian Federation under contract No.14.W03.31.0032.

\*Corresponding author: [radion@appl.sci-nnov.ru](mailto:radion@appl.sci-nnov.ru)

1. F. Vagizov, The splitting of hyperfine lines in  $^{57}\text{Fe}$  nuclei in RF magnetic field, *Hyperfine Interactions*, **61**, 1359-1362 (1990).
2. P. Helisto, I. Tittonen, M. Lippmaa, T. Katila, Gamma echo, *Phys. Rev. Lett.* **66**, 2037-2040 (1991).
3. Yu. V. Shvyd'ko, T. Hertrich, U. van Bürck, E. Gerdau, O. Leupold, J. Metge, H. D. Rüter, S. Schwendy, G. V. Smirnov, W. Potzel, and P. Schindelmann, Storage of Nuclear Excitation Energy through Magnetic Switching, *Phys. Rev. Lett.* **77**, 3232-3235 (1996).
4. R. Coussement, Y. Rostovtsev, J. Odeurs, G. Neyens, H. Muramatsu, S. Gheysen, R. Callens, K. Vyvey, G. Kozyreff, P. Mandel, R. Shakhmuratov, and O. Kocharovskaya, Controlling Absorption of Gamma Radiation via Nuclear Level Anticrossing, *Phys. Rev. Lett.* **89**, 107601 (2002).
5. R. N. Shakhmuratov, F. Vagizov, J. Odeurs, and O. Kocharovskaya, Slow  $\gamma$ -photon with a doublet structure: Time delay via a transition from destructive to constructive interference of collectively scattered radiation with the incoming photon, *Phys. Rev. A* **80**, 063805 (2009).
6. B. W. Adams, C. Buth, S. M. Cavaletto, J. Evers, Z. Harman, C. H. Keitel, A. Pálffy, A. Picón, R. Röhlberger, Yu. Rostovtsev, K. Tamasaku, X-ray quantum optics. *J. Mod. Opt.* **60**, 2–21 (2013).
7. S. Shwartz, R. N. Coffee, J. M. Feldkamp, Y. Feng, J. B. Hastings, G. Y. Ying, and S. E. Harris, X-Ray Parametric Down-Conversion in the Langevin Regime, *Phys. Rev. Lett.* **109**, 013602 (2012).
8. R. Röhlberger, H-C. Wille, K. Schlage, and B. Sahoo, Electromagnetically induced transparency with resonant nuclei in a cavity, *Nature* **482**, 199–203 (2012).
9. R. Röhlberger, K. Schlage, B. Sahoo, S. Couet, and R. Ruffer, Collective Lamb shift in single-photon superradiance, *Science* **328**, 1248–1251 (2010).

10. K. P. Heeg, et al., Vacuum-assisted generation and control of atomic coherences at x-ray energies, *Phys. Rev. Lett.* **111**, 073601 (2013).
11. R. Shakhmuratov, F. Vagizov, and O. Kocharovskaya, Single  $\gamma$ -photon revival and radiation burst in a sandwich absorber, *Phys. Rev. A* **87**, 013807 (2013).
12. K. P. Heeg, C. Ott, D. Schumacher, H.-C. Wille, R. Röhlsberger, T. Pfeifer, and J. Evers, Interferometric phase detection at x-ray energies via Fano resonance control, *Phys. Rev. Lett.* **114**, 207401 (2015).
13. K. P. Heeg, J. Haber, D. Schumacher, L. Bocklage, H.-C. Wille, K. S. Schulze, R. Loetzsch, I. Uschmann, G. G. Paulus, R. Ruffer, R. Röhlsberger, J. Evers, Tunable Subluminal Propagation of Narrow-band X-Ray Pulses, *Phys. Rev. Lett.* **114**, 203601 (2015).
14. K. P. Heeg, A. Kaldun, C. Strohm, P. Reiser, C. Ott, R. Subramanian, D. Lentrodt, J. Haber, H.-C. Wille, S. Goerttler, R. Ruffer, C. H. Keitel, R. Röhlsberger, T. Pfeifer, J. Evers, Spectral narrowing of x-ray pulses for precision spectroscopy with nuclear resonances, *Science* **357**, 375-378 (2017).
15. J. Haber, X. Kong, C. Strohm, S. Willing, J. Gollwitzer, L. Bocklage, R. Ruffer, A. Pálffy, and R. Röhlsberger, Rabi oscillations of x-ray radiation between two nuclear ensembles, *Nature Photonics*, **11**, 720-725 (2017).
16. J. Gunst, C. H. Keitel, and A. Pálffy, Logical operations with single x-ray photons via dynamically-controlled nuclear resonances, *Scientific Reports* **6**, 25136 (2016).
17. Wen-Te Liao, C. H. Keitel, and A. Pálffy, X-ray-generated heralded macroscopical quantum entanglement of two nuclear ensembles, *Scientific Reports* **6**, 33361 (2016).
18. Xiangjin Kong, A. Pálffy, Stopping Narrow-Band X-Ray Pulses in Nuclear Media, *Phys. Rev. Lett.* **116**, 197402 (2016).
19. F. Vagizov, V. Antonov, Y. V. Radeonychev, R. N. Shakhmuratov, and O. Kocharovskaya, Coherent Control of the Waveforms of Recoilless  $\gamma$ -Photons, *Nature* **508**, 80-83 (2014).
20. R. N. Shakhmuratov, F. G. Vagizov, V. A. Antonov, Y. V. Radeonychev, M. O. Scully, and O. Kocharovskaya, Transformation of a single-photon field into bunches of pulses, *Phys. Rev. A* **92**, 023836 (2015).
21. Y. V. Radeonychev, V. A. Antonov, F. G. Vagizov, R. N. Shakhmuratov, and O. Kocharovskaya, Conversion of recoilless  $\gamma$ -radiation into a periodic sequence of short intense pulses in a set of several sequentially placed resonant absorbers, *Phys. Rev. A* **92**, 043808 (2015).
22. V. A. Antonov, Y. V. Radeonychev, and O. Kocharovskaya,  $\gamma$ -ray-pulse formation in a vibrating recoilless resonant absorber, *Phys. Rev. A* **92**, 023841 (2015).
23. F. J. Lynch, R. E. Holland, and M. Hamermesh, Time dependence of resonantly filtered gamma rays from  $\text{Fe}^{57}$ , *Phys. Rev.* **120**, 513-520 (1960).

24. S.M. Harris, Quantum mechanical calculation of Mössbauer transmission, *Phy. Rev.* 124, 1178-1185 (1961).
25. E. Ikonen, P. Helistö, T. Katila, and K. Riski, Coherent transient effects due to phase modulation of recoilless gamma radiation, *Phys. Rev. A* **32**, 2298-2315 (1985).
26. G.V. Smirnov, General properties of nuclear resonant scattering, *Hyperfine Interactions*, **123/124**, 31-77 (1999).
27. Yu. V. Shvyd'ko, and G. V. Smirnov, Enhanced yield into the radiative channel in Raman nuclear resonant forward scattering, *J. Phys. Condens. Matter* **4**, 2663, (1992).
28. L.T. Tsankov, The spectrum of Mössbauer radiation passed through a vibrating resonant medium, *J. Phys. A.: Math., Nucl. Gen.* 13, 2959, (1980).
29. M. D. Crisp, Propagation of Small-Area Pulses of Coherent Light through a Resonant Medium, *Phys. Rev. A* 1, pp. 1604-1611 (1970).
30. M. J. Berger, J.H. Hubbell, S. M. Seltzer, J. Chang, J. S. Coursey, R. Sukumar, D. S. Zucker, and K. Olsen, *XCOM Photon Cross Sections Database (version 1.5)* (National Institute of Standards and Technology, Gaithersburg, MD, 2010), Online Available: <http://physics.nist.gov/xcom>.
31. B.P. Sorokin, G.M. Kvashnin, A.P. Volkov, V.S. Bormashov, V.V. Aksenkov, M.S. Kuznetsov, G.I. Gordeev, and A.V. Telichko, AlN/single crystalline diamond piezoelectric structure as a high overtone bulk acoustic resonator, *Appl. Phys. Lett.* 102, 113507 (2013).
32. A. Ambrosy and K. Holdik, Piezoelectric PVDF films as ultrasonic transducers, *J. Phys. E: Sci. Instrum.* 17, 856 (1984).



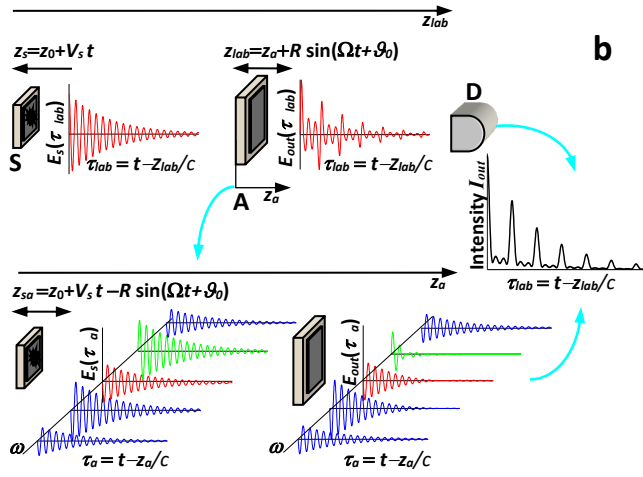


Fig. 1. (Color online) (a) Energy diagram in the left side of this figure illustrates a decay of  $^{57}\text{Co}$  nucleus with a half-life of  $T_{1/2} \approx 272$  days from the state  $|d\rangle$  to the state  $|c\rangle$ , followed by a cascade decay:  $|c\rangle \rightarrow |b\rangle$  and  $|b\rangle \rightarrow |a\rangle$  with emission of a 122 keV and 14.4 keV photons (shown by blue and red lines, respectively). Energy diagram in the right side of this figure shows the quantum transition in  $^{57}\text{Fe}$  nucleus from the ground state  $|1\rangle$  to the excited state  $|2\rangle$  induced by a recoilless 14.4 keV photon.

(b) Illustration of the experiment [19] for transformation of the exponentially decaying single-photon waveform into the regular pulse sequence in the laboratory reference frame (upper part) and in the reference frame of the vibrating absorber (lower part). Radioactive source “S” (a foil with  $^{57}\text{Co}$  radionuclide) emits 14.4 keV recoilless  $\gamma$ -ray photon (red pulse). A stainless steel foil “A” with  $^{57}\text{Fe}$  nuclei vibrates in the laboratory reference frame along the propagation axis  $z_{lab}$  according to (3). The source is uniformly moved at velocity  $V_s$  to properly shift the carrier frequency of the photon with respect to the resonance frequency of the absorber due to the Doppler effect. At the exit from the absorber quasi-monochromatic single-photon wave packet turns into regular pulse train. Its waveform is registered by detector “D”. This effect has clear interpretation in the reference frame co-moving with the absorber (lower part). In the absorber reference frame a field of the emitted photon looks as a set of quasi-monochromatic components described by Eq.(5c). All components are phase-locked except for one antiphased component marked by a green color. Due to the uniform motion of the source, the antiphased (green) component is tuned to the resonance with an absorber’s transition. At the exit from the absorber it is strongly attenuated and transformed into the dynamical beats. Influence of the absorber resonance on the off-resonant components in optically deep absorber also leads to their dynamical beats [see Eqs.(19)]. Temporal interference of the output spectral components results in a pulsed photon’s waveform that is the same in both reference frames (see the text).

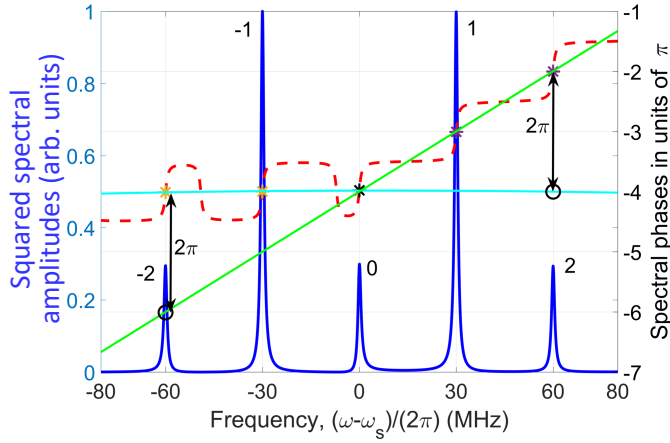


Fig. 2. (Color online) Fourier transform of the incident photon field, emitted by  $^{57}\text{Co}$  radioactive source, in the reference frame of the oscillating  $^{57}\text{Fe}$  absorber. The photon energy is  $\hbar\omega_s = 14.4$  keV. The bandwidth of each sideband is  $\Gamma_s/(2\pi) = 1.13$  MHz. The frequency of absorber's vibration is  $\Omega/(2\pi) = 40$  MHz. The initial phase of vibration is  $\mathcal{G}_0 = 0$ . The initial phase of the photon field is  $\varphi_0 = 0$ . The bold blue solid line corresponds to the squared modulus of spectral amplitude of the field, while bold dashed red line shows its spectral phase. The phases at the central frequencies (central phases) of the (a) -2<sup>nd</sup> and -1<sup>st</sup>, (b) 0<sup>th</sup>, and (c) 1<sup>st</sup> and 2<sup>nd</sup> spectral components are shown by (a) orange, (b) black, and (c) lavender asterisks, respectively. The central phases of the -2<sup>nd</sup> and 2<sup>nd</sup> sidebands, shifted by  $-2\pi$ , are shown by black circles. The central phases of the -2<sup>nd</sup>, -1<sup>st</sup>, 0<sup>th</sup> and 2<sup>nd</sup> spectral components are aligned along the light dash-dotted cyan horizontal line, while the central phases of the -2<sup>nd</sup>, 0<sup>th</sup>, 1<sup>st</sup> and 2<sup>nd</sup> spectral components are aligned along the light dash-dotted green diagonal line.

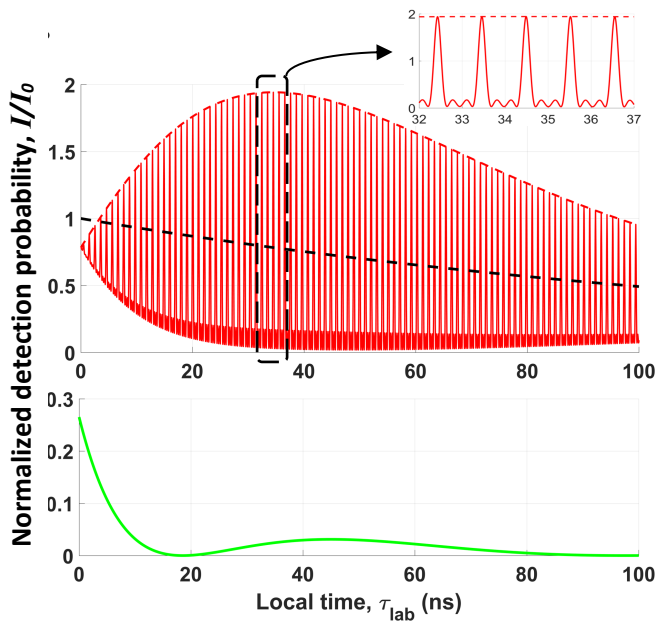


Fig. 3. (Color online) Time dependence of the photon detection probability,  $I_{out}(\tau_{lab})$ , normalized to the peak detection probability of the photon at the absorber entrance,  $I_0$ , (red pulses) for the vibration frequency 970 MHz corresponding to the analytical solution (21) that in this case practically coincides with general solution (18) at this vibration frequency. Tops of pulses are described by relation (23a). Red dashed curve is the pulse envelope,  $I_{out}^{peak}(\tau_{lab})$ , (23). Black dashed curve is the waveform of the incident photon. Green curve in a lower panel is the dynamical beats of the -1<sup>st</sup> sideband of the photon field (in the vibrating reference frame) plotted according to (22) for  $m=-1$ . Pulse duration is about 190 ps. Maximum of pulse height and the first hump of dynamical beats occur at  $\tau_{lab} \cong 35ns$  and  $\tau_{lab} \cong 46ns$ , respectively.

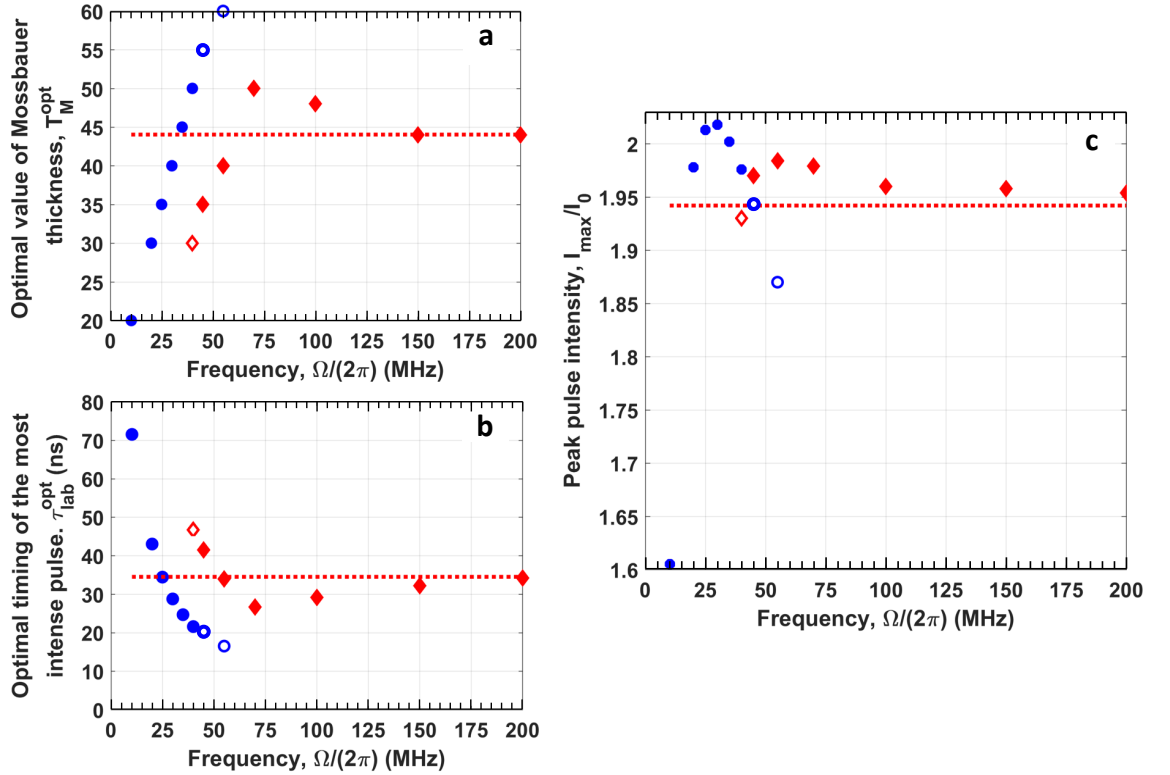


Fig. 4. (Color online) Vibration frequency dependencies of the optimal values of (a) Mössbauer thickness of the absorber,  $T_M^{opt}(\Omega)$ , and (b) the moment of formation of the highest pulse,  $\tau_{lab}^{opt}(\Omega)$ , as well as (c) of the corresponding intensity of the highest pulse,  $I_{max}(\Omega)/I_0$ , shown by filled marks at discrete frequency values with step multiple to 5 MHz. Blue and red filled and open marks are numerical optimization of Eq. (18), red dotted line is optimization (25) of the analytical solution (23). At  $\Omega/(2\pi) = 40, 45, 55$  MHz two values,  $T_M^{opt}$  and  $T_M'$  in (a) as well as  $\tau_{lab}^{opt}$  and  $\tau_{lab}'$  in (b) are shown by filled and open marks, respectively. These values correspond to the maximum peak pulse intensity,  $I_{max}/I_0$  [the respective filled marks in (c)] and to the lower

maximum,  $I'_{\max}/I_0$  [the respective open marks in (c)] which appears at frequency  $\Omega/(2\pi) \approx 35\text{MHz}$  and disappears at  $\Omega/(2\pi) \approx 75\text{MHz}$  (having values out of the displayed region). For example, at frequency  $\Omega/(2\pi) = 45\text{MHz}$  the first (from the left) filled red rhombs in (a) and (b) label values  $T_M^{opt} \approx 35$  and  $\tau_{lab}^{opt} \approx 41.5\text{ns}$ , respectively corresponding at this frequency to the maximum peak pulse intensity  $I_{\max}/I_0 = 1.97$  [also labeled by the filled red rhomb in (c)]. The lower value,  $I'_{\max}/I_0 \approx 1.94$ , in (c) corresponds to  $T'_M \approx 55$  in (a) and  $\tau'_{lab} \approx 20\text{ns}$  in (b) and is labeled by open circles. More detailed discussion is given in the text and in Fig. 5b.

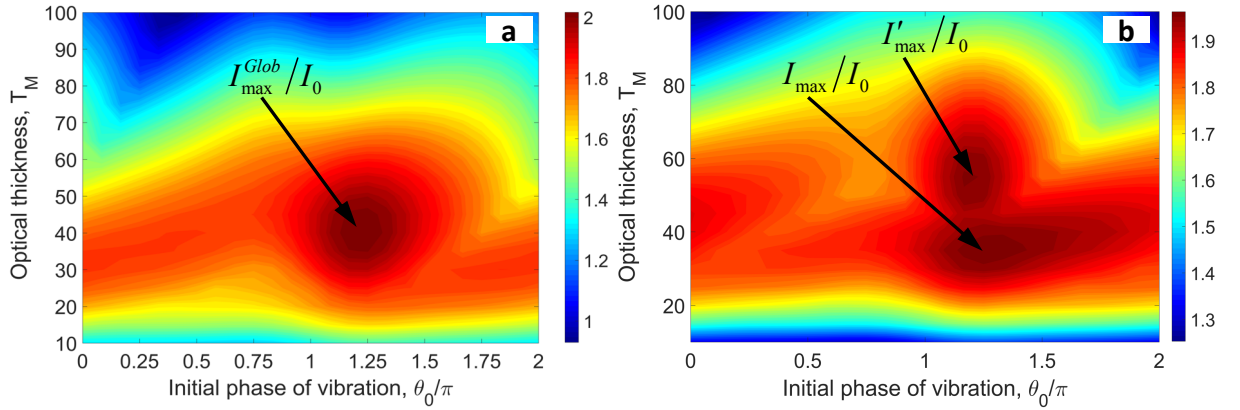


Fig. 5. (Color online) Peak detection probability of the photon, normalized to peak detection probability at the absorber entrance,  $I_{out}^{peak}(T_M, \tau_{lab}^*, \mathcal{G}_0)/I_0$  (where  $\tau_{lab}^* \equiv \tau_{lab}(T_M, \mathcal{G}_0)$  corresponds to the top of the highest pulse) versus the Mössbauer thickness,  $T_M$ , and the initial phase of absorber's vibration,  $\mathcal{G}_0$  at the determined value of  $\Omega$ . The calculations are based on Eq. (18) where the  $-1^{\text{st}}$  sideband of the photon field is tuned to the resonance ( $m = -1$  and  $\omega_s - \omega_a = \Omega$ ). The frequency of vibration is  $\Omega/(2\pi) = 30\text{MHz}$  for (a) and  $\Omega/(2\pi) = 45\text{MHz}$  for (b). The maximum value for (a) is  $I_{\max}^{Glob}/I_0 \approx 2.02$  achieved at  $T_M^{Glob} \approx 40$ ,  $\mathcal{G}_0^{Glob} \approx 5\pi/4$  and  $\tau_{lab}^* = \tau_{opt}^{Glob} \approx 28\text{ns}$ . In the case (b) there are two maxima:  $I_{out}^{peak}(T_M, \tau_{lab}^*, \mathcal{G}_0)/I_0 = I_{\max}/I_0 \approx 1.97$  (see also Fig.4c, the first filled red rhomb) is achieved at  $T_M = T_M^{opt} \approx 35$  (see also Fig.4a, the first filled red rhomb),  $\mathcal{G}_0 \approx 5\pi/4$ , and  $\tau_{lab}^* = \tau_{lab}^{opt} \approx 41.5\text{ns}$  (see also Fig.4b, the first filled red rhomb); as well as  $I_{out}^{peak}(T_M, \tau_{lab}^*, \mathcal{G}_0)/I_0 = I'_{\max}/I_0 \approx 1.94$  (see also Fig.4c, the first open circle), achieved at  $T_M = T'_M \approx 55$  (see also Fig.4a, the first open circle),  $\mathcal{G}_0 \approx 5\pi/4$ , and  $\tau_{lab}^* = \tau'_{lab} \approx 20\text{ns}$  (see also Fig.4b, the first open circle).

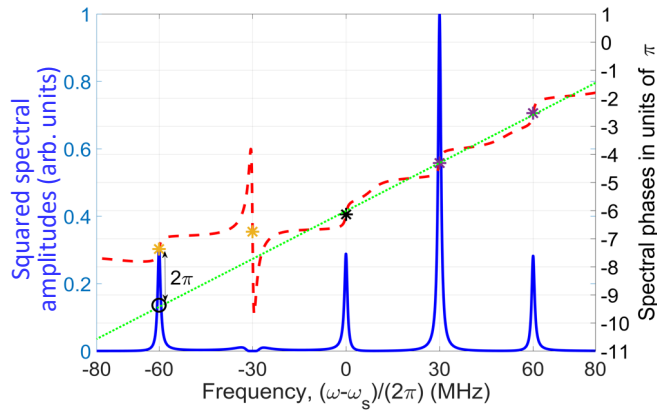


Fig. 6. (Color online) The same as in Fig. 2, but after transmission of the photon through the resonant absorber tuned to the resonance with the  $-1^{\text{st}}$  sideband of the photon field, under the global optimum conditions:  $I_{\text{max}}^{\text{Glob}}/I_0 \simeq 2.02$ ,  $\Omega/(2\pi) = 30$  MHz,  $T_M^{\text{Glob}} = 40$ , and  $\mathcal{G}_0^{\text{Glob}} = 5\pi/4$ . The spectrum corresponds to blue curve in Fig. 7.

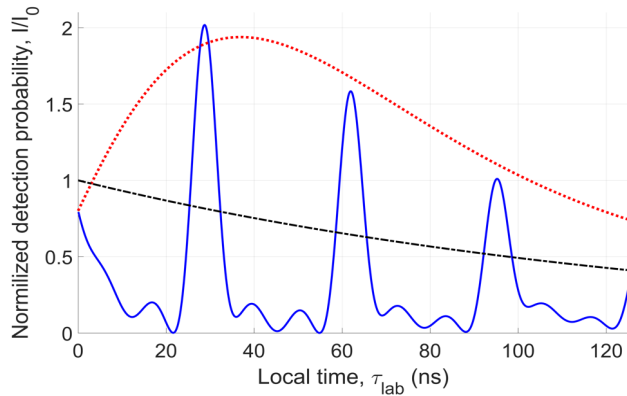


Fig. 7. (Color online) Time dependence of the photon detection probability normalized to the peak detection probability of the photon at the absorber entrance,  $I_0$ , corresponding to the spectrum in Fig. 6. Blue solid curve shows the general solution (18). Pulse duration is about 6 ns. Black dash-dotted curve is the waveform of the incident photon. Red dotted curve shows the analytical solution for the pulse envelope (23) at the same parameter values but accounting for the dynamical beats of the  $-1^{\text{st}}$  sideband only.

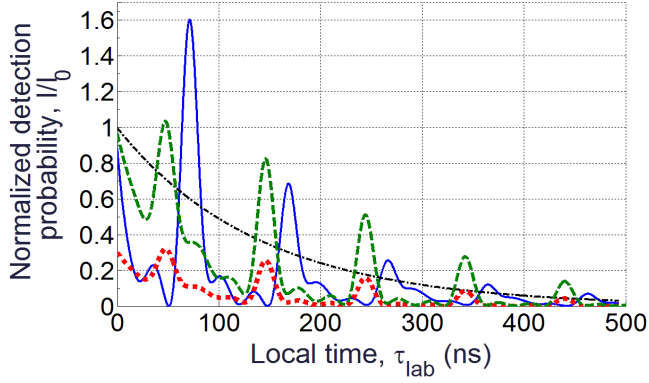


Fig. 8. (Color online) Time dependence of detection probability of  $\gamma$ -ray photon transmitted through vibrating stainless steel foil. The frequency of vibration for all curves is  $\Omega/(2\pi) = 10.2$  MHz. Red dotted curve corresponds to the parameter values used in the experiment [19]:  $T_M = 5.2$ ,  $\mathcal{G}_0 = 0$ , natural abundance, 2.2%, of  $^{57}\text{Fe}$  in iron fraction. Green dashed curve is plotted at the same parameter values but for 90% of  $^{57}\text{Fe}$  in iron fraction. Blue solid curve is the result of optimization: 90% of  $^{57}\text{Fe}$  in iron fraction,  $T_M = 17.5$ ,  $\mathcal{G}_0 = 1.35\pi$ . The absorber is tuned to resonance with the -1<sup>st</sup> sideband of the photon field in the oscillating reference frame. Black dash-dotted curve is the waveform of the incident photon at the absorber entrance.

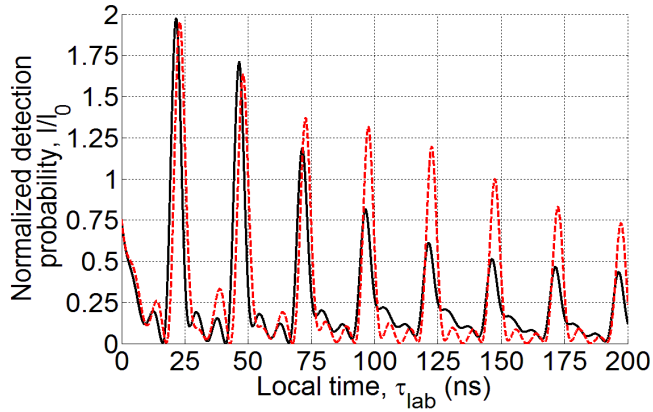


Fig. 9. (Color online) Output photon waveforms in the cases of (i) suppression of the -1<sup>st</sup> sideband of the photon field via its resonant absorption (black solid line) and (ii)  $\pi$  phase-shift of the -1<sup>st</sup> sideband via the resonant dispersion (red dashed line). The frequency of vibration is  $\Omega/(2\pi) = 40$  MHz. Highest excess of the red curve over the black one is achieved for the pulse centered at  $\tau_{lab} \approx 122.6$  ns.

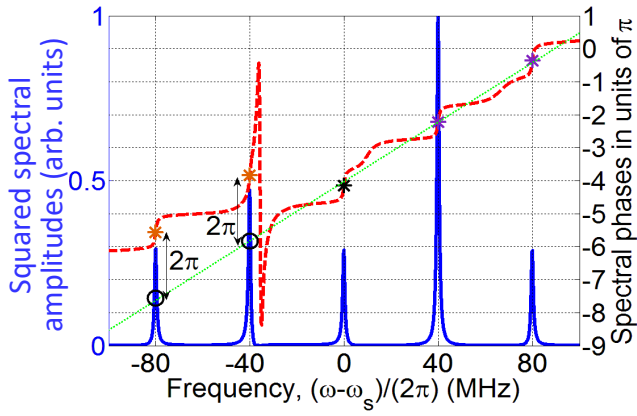


Fig. 10. (Color online) The same as in Fig. 2, but after transmission of the photon through the resonant absorber. The absorber parameters:  $T_M = 50$ ,  $\mathcal{G}_0 = 7\pi/6$ , and  $\Delta\omega_{-1} = 4.4$  MHz are chosen in such a way that the photon field at the central frequency of the -1<sup>st</sup> sideband acquires a  $\pi$  phase-shift. All (five) the considerably nonzero spectral components of the output photon field are phase-aligned.

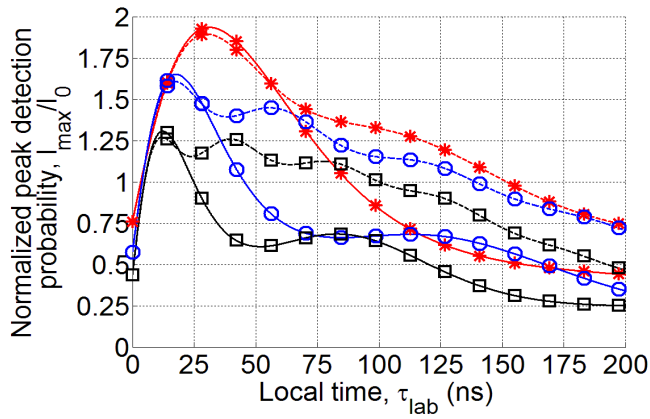


Fig. 11. (Color online) Envelopes of the pulse trains, corresponding to the output photon waveforms, produced via absorption of the -1<sup>st</sup> sideband of the photon field (solid lines) and via its  $\pi$  phase-shift (dashed lines). The frequency of absorber's vibration is  $\Omega/(2\pi) = 40$  MHz. Red color and stars correspond to the curves plotted for  $T_M = 50$ , blue color and circles indicate the curves, plotted for  $T_M = 100$ , black color and squares mark the curves, corresponding to  $T_M = 150$ .